1
Introduction

Molecular motions in fluids are of long-standing interest to physicists, chemists, materials engineers, and biologists since the dynamics bear a direct relationship to the physical and rheological properties underlying many applications. A first-principles approach to understanding material properties would address how the chemical structure determines the forces between molecules, and in turn how these forces govern the molecular motions. Fluctuation-dissipation theory then provides a connection between theoretical models and experimental observables. The latter usually involve the decay of stress, polarization, or other measurable quantities, which are the macroscopic manifestation of the molecular diffusions, reorientations, and conformational transitions returning the perturbed system to equilibrium.

The relaxation[1] of even simple van der Waals fluids remains a continuing field of study. Analysis of liquid motions is simplest for non-interacting species, and solutions were obtained in the early twentieth century for translational Brownian diffusion[2] [1] and rotational diffusion [2] in dilute solution. For viscous liquids of sufficient density that molecules exert a reciprocal influence, mutual interactions can dominate the behavior – neighboring species must make small adjustments in position in order for a given molecule to change configuration. The behavior deviates from thermally excited transitions between potential wells, and theoretical efforts to describe the many-body dynamics remain largely at the model-building stage. It is in the study of such complex correlated dynamics that polymers in general, but rubber in particular, can be most useful – the former because of their diverse properties, unique phenomena, and facile supercooling;[3] the latter because only rubber among polymers exists in a state of structural and mechanical equilibrium. For this reason, rubber is the most fundamentally interesting polymeric material. Its unique properties have also led to wide application in industry, the military, and for consumer products (world consumption of natural and synthetic rubber exceeded 23 million tons in 2008 [3]), which in turn has spurred further research.

[1] The term "relaxation" is used to describe both the experimental data (e.g., relaxation spectra) and the underlying motions (e.g., segmental relaxation times).

[2] Thermally driven random movement of molecules is known as Brownian motion, after the 1827 Scottish botanist Robert Brown, who used a microscope to observe the irregular paths followed by pollen particles suspended in water. Initially ascribed to the particles being alive, the correct mechanism – molecular collisions – was identified by Einstein in 1905. Living cells also exhibit migration, but the motion is well beyond that due to thermal fluctuations.

[3] Traditionally "supercooling" referred to quenching below the melting point to a metastable liquid state; however, many polymers are incapable of crystallization due to irregularity of their chemical repeat units and thus have no melting temperature. Nevertheless, reducing their temperature towards the glass transition is still regarded as supercooling.

1.1 Viscoelasticity and high elasticity in polymers

The distinctive feature of polymers is the enormous size of the constituent molecules ("macromolecules"), which can be two orders of magnitude larger than the distance between segments. This is quite different from ordinary liquids, which, unless near a critical point or the glass transition, have only one characteristic length scale, the intermolecular separation, equal to a few Angstroms. It is the size and consequent large aspect ratio of chain molecules that give polymer melts[4] (that is, amorphous polymers above the glass-transition temperature T_g) their special properties, in particular high elasticity and viscoelasticity.

High elasticity (rubber elasticity) refers to the ability of flexible-chain polymers to recover from large strains, a property unique to chain molecules. Experiments have shown that high molecular weight, uncrosslinked polymers exhibit recoverable strains (stretched length divided by length after recovery) of as much as 10 [4,5]. Entanglements give rise to a transient network that responds to applied forces through conformational changes of the polymer backbone (e.g., for extensional strains *gauche* rotamers convert to the more extended *trans* form). The rotations of backbone segments are highly correlated (intramolecular cooperativity) to avoid large displacements of the chain. Upon removal of the external force, the material recovers some of its original dimensions since the conformational transitions are reversible. High elastic strains are attained in polymeric liquids only if the strain rate is large relative to the molecular response time; flow, which changes the relative position of the molecules, leads to unrecovered strain ("set"). A network of chemically bonded chains, however, retains it shape, with any permanent set the result of defects, chain scission, or mechanically labile network junctions. As implied by the name, permanent set is distinct from recoverable strain that may be retarded due to the viscoelastic nature of polymers. This behavior is discussed in Chapter 4.

A measure of the hypothetical maximum extension of a polymer chain is the ratio of its fully extended length to its mean length. From eqn. (1.22) below, this quantity is proportional to the square root of the number of backbone bonds. For a typical polymer having a molecular weight $\sim 10^5$ g/mol ($\sim 10^3$ repeat units), this extension is on the order of 100. Of course, reversible strains this large are unattainable for real networks, which are limited by defects and finite extensibility.

Viscoelasticity describes a time-varying reaction to a transient perturbation in an unchanging material; equivalently, the perturbation could be dynamic, resulting in a frequency-dependent response. The requirement is that the response changes with time even though the material does not. Viscoelasticity includes mechanical properties such as stress relaxation and the dynamic modulus, as well as experimental quantities involving related molecular motions, such as dielectric polarization and the quasi-elastic scattering of light, X-rays, or neutrons. The term itself implies a second, equivalent definition: energy is both dissipated and stored during deformation of a viscoelastic material; that is, the material response has viscous and elastic components.

Non-polymeric materials exhibit viscoelastic effects, a prominent example being supercooled small-molecule liquids [6,7]. Viscoelasticity is manifested in metals as creep under

[4] "Melt" is commonly used for high molecular weight, amorphous polymers above T_g, with the term liquid reserved for unentangled polymers; this distinction reflects the fact that entanglements confer solid-like properties over a limited frequency range. However, the terminology is confusing insofar as "melt" implies the loss of an ordered structure, such as found in crystals. Since near T_g the viscoelastic behaviors of molecular liquids and polymer melts are indistinguishable, the terms are used interchangeably herein.

sustained loading [8] and becomes significant at temperatures above about 0.5 times their melting point [9]. This high-temperature creep is due to changes in the microstructure of the metal, but even well below the melting point metals are not entirely elastic. For example, long term creep in the Cu-Be wires of a torsional balance introduced small errors into measurements of the gravitational constant [10]. Strictly speaking, the behavior of metals is not truly viscoelastic, since the changing response to a load is usually caused by changes in the material itself, e.g., its dislocation structure or grain size.

Polymers are the prototypical viscoelastic materials, exhibiting large rate dependences at almost all temperatures. The normal forces accompanying shear flow of polymers is another consequence of their viscoelasticity (although normal stresses are not unique to viscoelastic fluids). Viscoelasticity is a consequence of the diverse range of molecular motions in polymers, which means that for any applied stress or strain, some relaxation modes are moving on the timescale of the perturbation and thereby dissipating energy. This gives rise to a peak in the out-of-phase, or loss, component of the dynamic response, at a frequency equal to the frequency of the underlying molecular motions. Other modes, moving relatively fast, respond either elastically or, for the entire molecule in the absence of crosslinking, as flow. Some molecular motions may have very long time constants, so as to be "frozen" or unresponsive, on the timescale of the perturbation; an example would be conformational transitions of the polymer backbone below T_g. In rheology two parameters are used to describe the competition between the timescale of the imposed perturbation and the time characterizing the material response. The Deborah number[5] is the ratio of the response time to the experimental timescale. A large Deborah number means the fluid responds in a more solid-like fashion. The related Weissenberg number[6] is the ratio of the material relaxation time to the process time during flow, and is used to characterize the amount of molecular orientation induced by the flow.

In Figure 1.1 the in-phase and out-of-phase components of the dynamic modulus are shown for high molecular weight 1,4-polyisoprene (PI) subjected to a periodic shear strain [11]. The energy stored per cycle is proportional to the storage modulus, G', and the energy dissipated to the loss modulus, G''. Energy storage and loss are both expected whenever relaxation occurs, although the two quantities are not independent. According to the Kramers–Kronig relation [12], based on the principle of causality (the time order of cause and effect)

$$\int_0^\infty G'(\omega)\,\frac{\sin\omega t}{\omega}\,d\omega = \int_0^\infty G''(\omega)\,\frac{\cos\omega t}{\omega}\,d\omega = \frac{\pi}{2}\,G(t) \tag{1.1}$$

where $G(t)$ is the stress relaxation modulus measured in a transient experiment and ω is the circular frequency, equal to 2π times ν, the frequency in Hertz. Although valid for all linear responses, eqn (1.1) is difficult to apply because it requires knowledge of the modulus function over the entire frequency range. There are various approximations to the Kramers–Kronig relation [13], for example

$$G''(\omega) \approx \frac{\pi}{2}\frac{dG'(\omega)}{d\,\ln\omega} \tag{1.2}$$

[5] The term comes from the biblical quote by the prophetess Deborah *"The mountains melted from before the Lord"* (Judges 5:5, KJV).

[6] Named for the early twentieth century Austrian rheologist Karl Weissenberg.

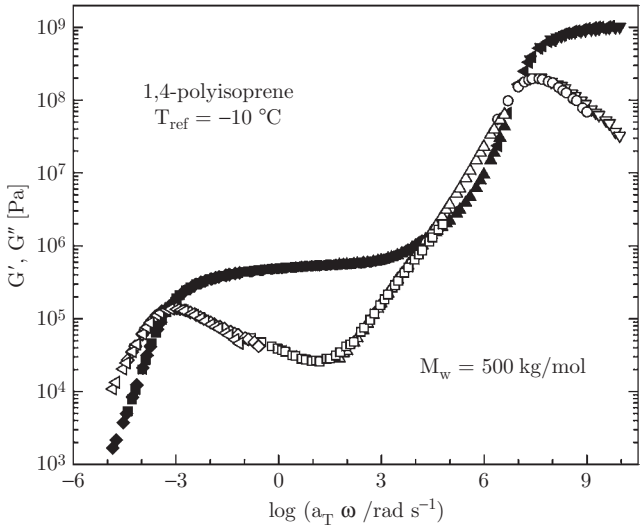

Figure 1.1 Dynamic storage and loss modulus of polyisoprene ($M_w = 500$ kg/mol). The symbols denote the different measurement temperatures, with the isotherms shifted to obtain the master curve at the indicated reference temperature. The spectra exhibit both aspects of viscoelasticity – the modulus varies with frequency and the response has both elastic and dissipative components. Data from ref. [11].

The corresponding equation for the dielectric loss is sometimes used to circumvent the masking of loss peaks by ionic conductivity, since the latter does not contribute to the in-phase response [14].

The frequency of molecular motions is characterized by a time constant or relaxation time. The classical definition is the time required for the perturbation to be reduced by a factor of e ($\sim$2.72). This implies exponential decay (or Debye relaxation in the frequency domain), which is valid for relaxation that is homogeneous and proceeds at a rate proportional to the amount remaining to relax. For example, after imposition of a strain, the stress, $\sigma(t)$, relaxes according to

$$\frac{d\sigma}{dt} = -k_0\sigma(t) \tag{1.3}$$

$$\sigma(t) = \sigma_0 \exp(-k_0 t) \tag{1.4}$$

where σ_0 is the initial stress and k_0 the rate constant (equal to the reciprocal of the relaxation time). Exponential relaxation rarely describes the intermolecularly cooperative motions in dense fluids. Another characteristic timescale is the period required for complete cessation of the decay; however, this is usually too long to be practical and relies on judgment of when equilibrium has been reestablished. (Since variables still fluctuate while in thermal equilibrium, an indicator that equilibrium has been attained is when the change of a variable with time becomes equal to its rate of change due only to equilibrium fluctuations [15].)

An absorption peak in the loss modulus (Figure 1.1) or dielectric loss, reflecting the conversion of mechanical or electrical energy to heat, can be used to define a model-independent, most probable relaxation time as the reciprocal of the peak frequency, $\tau_{max} = \omega^{-1}$. If the peak in the spectrum is symmetric, τ_{max} is also the mean relaxation time. However,

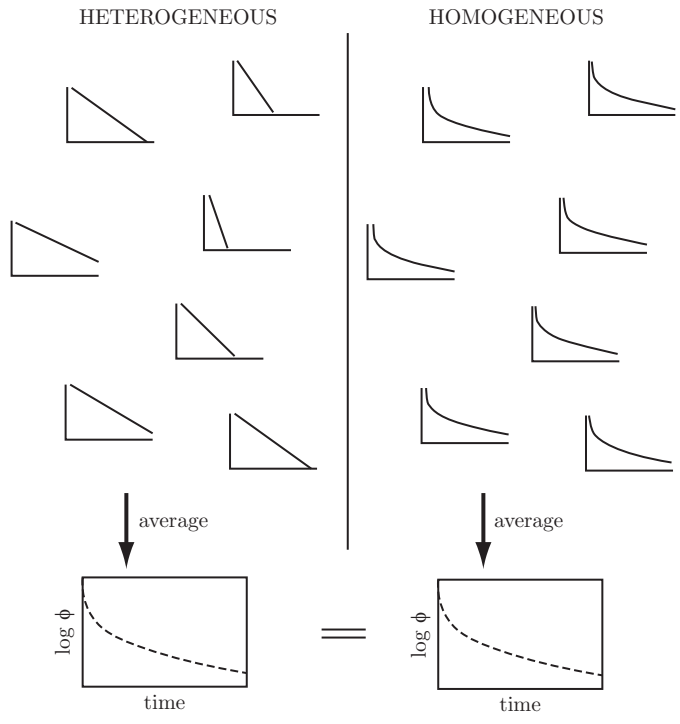

Figure 1.2 Heterogeneous and homogeneous dynamics leading to non-exponential relaxation. The former corresponds to a distribution of exponential relaxation times and the latter to inherently non-exponential relaxation function. The spatially distributed responses are averaged to yield the observed decay function, which is indistinguishable for the two scenarios. Reproduced from ref. [17] with permission.

relaxation functions are often asymmetrically broadened. The asymmetry can arise due to heterogeneous relaxation, in which the response is a weighted summation of simple exponential decays

$$G(t) \sim \int_{-\infty}^{\infty} H(\tau) e^{-t/\tau} d(\ln\tau) \tag{1.5}$$

with $H(\tau)$ the distribution function. Alternatively, the relaxing species may just decay in an inherently non-exponential fashion, in which an empirical equation or a model is used to describe the peak shape. An $H(\tau)$ can always be found that will fit the data, with the mean relaxation time given by the weighted sum

$$\langle\tau\rangle = \frac{\int_0^{\infty} \tau H(\tau)}{\int_0^{\infty} H(\tau)} d\tau \tag{1.6}$$

Since molecular motions in polymers encompass such a broad frequency range, a logarithmic timescale is more useful; that is, the distribution is expressed in terms of $\ln\tau$ ($d\ln\tau = \tau^{-1} d\tau$) [16]. Heterogeneous and homogeneous relaxation scenarios are depicted in Figure 1.2 [17].

A common form of asymmetry of relaxation peaks is characteristic skewing toward higher frequencies ("stretched exponential decay") that conforms in the time domain to the Kohlrausch function[7] [18,19]

$$G(t) = G_0 \exp[-(t/\tau_K)^{\beta_K}] \tag{1.7}$$

where G_0 is a constant and $0 < \beta_K \leq 1$. This equation is obtained by making the rate constant in eqn (1.3) time dependent: $k_0(t) \sim t^{\beta_K - 1}$. The one-sided Fourier transform of eqn (1.7) gives the Kohlrausch function in the frequency domain and, while written in terms of the mechanical modulus, there are corresponding equations for dielectric relaxation, quasi-elastic scattering, etc. If eqn (1.7) arises from a superposition of exponential relaxation functions

$$G(t) = \int_0^\infty H(\tau) \exp(-t/\tau) d\tau \tag{1.8}$$

the distribution of relaxation times is given by [20]

$$H_K(\tau) = -\frac{1}{\pi\tau} \sum_{k=0}^{\infty} \frac{(-1)^k}{k!} \sin(\pi\beta k) \Gamma(\beta k + 1) \tau^{\beta k} \tag{1.9}$$

where Γ is the gamma function.[8] This distribution function includes several decades of relaxation times shorter than the main (peak) relaxation time. Equation (1.9) must be evaluated numerically, although a good approximation is

$$H_K(\tau) \cong \left[\frac{\beta_K}{2\pi(1-\beta_K)\tau^2}\right]^{\frac{1}{2}} \left[\frac{\beta_K \tau}{\tau_K}\right]^{\frac{\beta_K}{2(1-\beta_K)}} \exp\left[-(1-\beta_K)\left(\frac{\beta_K \tau}{\tau_K}\right)^{\frac{\beta_K}{(1-\beta_K)}}\right] \tag{1.10}$$

The Kohlrausch relaxation time τ_K is related to the mean value as

$$\langle\tau\rangle = \frac{\tau_K}{\beta_K} \Gamma(\beta_K^{-1}) \tag{1.11}$$

Fitting the higher-frequency dispersion in Figure 1.1 to eqn (1.7) gives $\beta_K = 0.52$, with the full width at half-maximum (FWHM) = 2.11 decades. The lower limit for a dispersion is the breadth of a Debye peak (β_K is unity), FWHM = 1.144 decades. The various relaxation times for the segmental peak in Figure 1.1 are $\tau_K = 0.25$ μs, $\tau_{max} = 0.33$ μs, and $\langle\tau\rangle = 0.46$ μs; this rank ordering of magnitudes

$$\tau_K \leq \tau_{\max} \leq \langle\tau\rangle$$

is general and not specific to any particular value of β_K.

Exponential decay usually describes thermally excited single molecule transitions, expected to conform to an Arrhenius temperature dependence

$$\tau = \tau_\infty \exp(-E_a/RT) \tag{1.12}$$

[7] This function is also named after Williams and Watts, who derived it independently [19].

[8] The gamma function $\Gamma(x) = \int_0^\infty e^{-u} u^{x-1} du$. If x is a positive integer, $\Gamma(x) = (x-1)!$

with a constant activation enthalpy[9] E_a (R is the gas constant). A heuristic argument, referred to as the compensation rule, requires that the prefactor, τ_∞, in eqn (1.12) be related to E_a according to [21]

$$\tau_\infty \propto \exp(-E_a) + constant \tag{1.13}$$

If correct, a distribution of exponential decays would be invalid for many observed relaxation phenomena. However, non-exponential relaxation is rarely associated with Arrhenius behavior. If all molecular motions contributing to the response have the same temperature dependence, temperature alters only the timescale of the response and the material is thermorheologically simple; that is, the behavior conforms to the time–temperature superposition principle. This aspect of viscoelastic behavior is addressed in detail in Chapter 6.

1.2 Modes of motion

There are various length scales in polymers, in addition to the intersegment or intermolecular distance in common with molecular liquids: (i) the Rouse length scale (∼ couple of nm), which refers to the shortest distance over which the separation of chain segments has a Gaussian distribution; (ii) the entanglement distance (*ca.* 3 to 8 nm), referring to the effective distance a chain moves transversely to its contour before experiencing topological constraints due to the uncrossability of the chains. It is these entanglement constraints that confer high elasticity to uncrosslinked rubber; and (iii) the molecular size *per se* ($\leq$ 50 nm). Since the conformational arrangement of polymer chains exhibits a dynamic equilibrium and the lengths of different chains may not be the same (molecular weight polydispersity), the macromolecular size is expressly defined by moments. For linear chains the mean square end-to-end distance, $\langle r^2 \rangle$, is an obvious measure of size, while for branched or cyclic chains the distribution of segments around the mass center is more meaningful; thus, the mean square radius of gyration is proportional to the mean square distance between each of the n backbone atoms.

$$\langle R_g^2 \rangle = \frac{1}{2n^2} \sum (r_i - r_j)^2 \tag{1.14}$$

For freely jointed chains or for real linear polymers under Theta conditions,[10] $\langle r^2 \rangle = 6R_g^2$. The molecular size of polymers has an especially significant effect on their rheological properties. When crosslinked, the primary chain length becomes irrelevant, aside from a small influence on network properties (e.g., strength and hysteresis) affected by chain ends.

These length scales refer to the structure of the material. However, in condensed matter including polymers, molecules and segments rearrange at different rates, giving rise to heterogeneous dynamics and thus dynamic length scales. Some of the dynamic properties unique to polymers are manifested in the glassy or semicrystalline states, but they are most apparent in amorphous polymers above their glass-transition temperature. It is these conditions that define a "rubber," which refers to an amorphous, flexible chain, high polymer[11] above T_g. (An elastomer is a rubber that has been chemically crosslinked.) If the polymer backbone lacks

[9] In the chemical literature E_a is referred to as an activation energy but enthalpy is the more correct term for an isobaric process, given the potential for PV work.

[10] Chains in solution under Theta conditions have the same configuration as in the equilibrium melt state.

[11] The term "high polymer" implies a molecular weight sufficiently large that the chain ends have no effect on properties.

flexibility, it cannot undergo the conformational transitions required for high elasticity. A metric of chain flexibility is the persistence length, l_p, describing the distance over which bond orientations become uncorrelated. l_p is equal to the area under the correlation function describing the orientational correlation of backbone bonds

$$C(r) = \langle \tilde{u}(0) \cdot \tilde{u}(r) \rangle \tag{1.15}$$

where $\tilde{u}$ is a unit vector parallel to the bond, r runs along the polymer contour, and the brackets imply the scalar product averaged over all chains. For a completely flexible polymer l_p equals one bond length, and for a completely rigid rod it is equal to the chain length. Another way to distinguish flexible chains from rigid-rod polymers is by their crystallization behavior [22–24]. Without the ability to conformationally rearrange, rigid rods maximize their packing by aligning in parallel fashion to form extended-chain crystals. To minimize the loss of orientational entropy, however, chains with sufficient flexibility will back-fold during crystallization, and this absence of extended chain crystals can serve as a defining characteristic of flexible-chain polymers. Based on a very approximate lattice model, Flory concluded that 0.63 was the fraction of bent (*gauche*) bonds necessary for a chain to crystallize with back-folding and thus be considered a flexible macromolecule [22]. High-speed spinning and related technologies are routes to achieve extended-chain crystallization of flexible-chain polymers by reducing the transient concentration of *gauche* conformers during processing [25,26,27]. Extended-chain crystals form stronger, more dimensionally stable fibers because the back-folds are defects. This Flory approach to chain flexibility leads to another way to contrast flexible and rigid chains – from the size of the chain relative to the size of a completely flexible chain having the same number of repeat units. This characteristic ratio, C_n, is defined in eqn (1.24) below.

Another classification of dynamic properties is between those that are unaffected by chain length, and thus common to materials composed of small molecules and macromolecules, and molecular motions that are unique to polymers. The former are the more local modes, including the glass transition, since one cannot distinguish a polymer from a molecular liquid using only measurements around T_g. As discussed below the dependence of T_g on molecular weight is due to the presence of chain ends; this dependence is not a direct consequence of the long-chain character of the molecule. The chain ends in a high polymer are too sparse to affect T_g and other properties.

The broad range of length scales in polymers leads to a diversity of their dynamics: vibrations, the Boson peak, the nearly constant loss, secondary relaxations including both side group motions and the Johari–Goldstein process, structural relaxation (the glass transition), the Rouses modes, and the entangled dynamics. Only the last two are unique to polymers. In Figure 1.3 various dynamics are evident in the dielectric loss spectrum of 1,4-polybutadiene (PBD) [28]. Temperature is used as the abscissa in order that the processes, which encompass more than 12 decades of frequency, can be viewed together. In general we expect slower dynamic processes to be progressively less sensitive to chemical structure, since motion over longer length scales averages out the structural details.

1.2.1 Vibrations

Beginning around 10^{-14} s and sensibly independent of temperature, the fastest motions of atoms (i.e. neglecting electronic excitations) are vibrations, which change the instantaneous bond angles and lengths and occur even in the glassy state. These are not specific to polymers

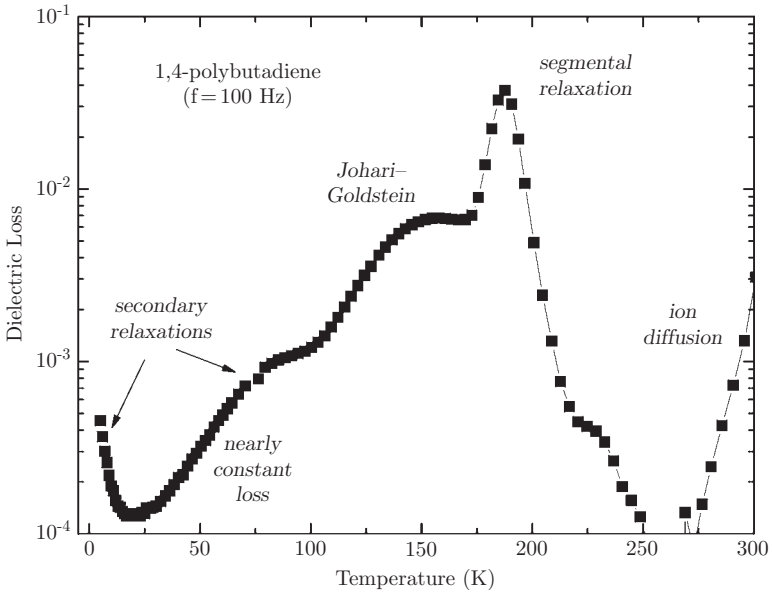

Figure 1.3 Dielectric loss of 1,4-polybutadiene measured as a function of temperature at 100 Hz. The different relaxation mechanisms appear as peaks, while the nearly constant loss and ionic conductivity are manifested as changes in slope. Data from ref. [28]

but do depend on the atoms and chemical structure; thus, vibrational spectroscopy is useful for identification of a material, including the polymer species and any additives. Related to these oscillations of individual moieties are the phonons. A universal feature of glassy and crystalline solids, phonon motion consists of lattice vibrations; i.e. collective modes in the form of extended plane waves. The term itself comes from the fact that long-wavelength phonons underlie the propagation of sound in solids. Phonon excitations transpire at very high frequencies, *ca.* 10^{12}Hz. The earliest model of phonons was due to Einstein, who assumed all vibrational frequencies to be equally probable [29]. This leads to incorrect predictions for the heat capacity of solids. A more accurate description of phonon motion is the Debye model, according to which elastic solids have a density of states $g(\omega)$ (number of states per unit frequency) proportional to ω^2 for ω less than a characteristic value known as the Debye frequency, $\omega_D \sim 10^{12}$ Hz. For frequencies greater than ω_D, $g(\omega) = 0$ [29,30]. Notwithstanding its simplicity the Debye model remains the starting point for treating low-temperature lattice vibrations. However, for disordered solids such as polymeric glasses, scattering experiments reveal an additional vibrational contribution, in excess of the Debye prediction. This excess $g(\omega)$ is seen as a maximum in $g(\omega)\omega^2$ at $\omega \sim 10^{12}$ Hz [31]. This so-called Boson peak, not observed in crystals, has a shape that is independent of chemical structure [32]. An example is shown in Figure 1.4 [33]. The origin of the Boson peak is much investigated, with the phenomenon of general interest because of the possibility that the Boson intensity correlates with properties of the liquid state including the glass transition [34–36].

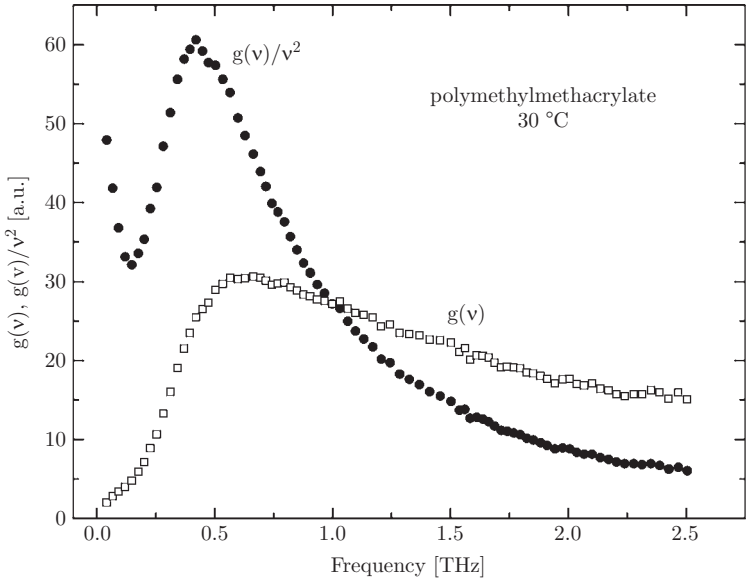

Figure 1.4 Vibrational density of states from the anti-Stokes Raman spectrum of PMMA, as measured (squares) and after division by ν^2 to make apparent the excess over the Debye theory. The spectrum is invariant to physical aging or thermal history. Data from ref. [33].

1.2.2 Nearly constant loss

Spectroscopic measurements on polymers such as PI [37], PBD [28,38], polyisobutylene (PIB) [39], polystyrene (PS) [39], and polymethylmethacrylate (PMMA) [40], as well as ions [41–45] and small molecules [46–49], reveal that the dynamics over a range of frequencies can be described by a slowly decreasing function of frequency, varying as $\omega^{-\lambda}$ where λ is a positive number close to zero. This is illustrated in light-scattering spectra for PIB both below and above T_g (Figure 1.5 [39]) and in dielectric spectroscopy on two PBDs, an oligomer and a higher molecular weight sample (Figure 1.6 [38]). Given the very weak frequency dependence, the process is referred to as the nearly constant loss (NCL). The frequency regime of the NCL is much higher than structural relaxation, so the response represents motion of species (ions, molecules, or chain segments) within the near-neighbor "cage." This cage confinement is responsible for the weak energy dissipation connoted by the term NCL.

Since the local liquid structure loosens with increasing temperature, the magnitude of the NCL increases with T (Figure 1.7); however, at higher T its temporal extent is reduced by encroachment on the low-frequency side from structural relaxation. For this reason the NCL is only observed at low temperatures and high frequencies. Thus, while the NCL should be ubiquitous, its detection is limited to conditions where there is no overlap with the more intense vibrational and reorientational contributions.

1.2.3 Secondary relaxations

Secondary relaxations are any of the myriad processes occurring at higher rates (or observed at lower temperatures) than the structural relaxation underlying the glass transition. The

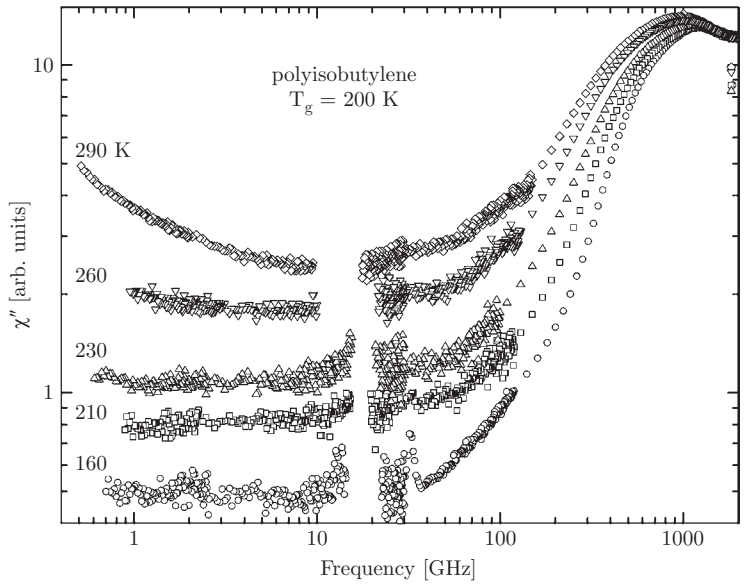

Figure 1.5 Depolarized light scattering susceptibility spectra for PIB, showing a flat, weakly T-dependent response around 1 to 30 GHz referred to as the NCL. The vibrational contribution to the spectra is evident at higher frequencies. Data from ref. [39].

most facile means to observe secondary relaxation peaks is dielectric spectroscopy because of its sensitivity and broad frequency range. Secondary relaxations are named using successive Greek letters beginning with β; the glass transition is the α-process. In Figure 1.8 dielectric spectra are shown for polycyclohexylmethacrylate, which has a complex structure and therefore multiple secondary processes. The relaxation times (inverse of peak frequency) corresponding to each process are shown in an Arrhenius plot in Figure 1.9 [50]. Secondary relaxations, found in small molecules as well as polymers, fall into two classes: the Johari–Goldstein (JG) relaxation and higher-frequency motions. The latter are more trivial, in the sense of being specific to a given material and generally having a limited effect on macroscopic, physical properties. The higher-frequency secondary relaxations are due to motion of some, but not all, atoms in the molecule or repeat unit. Examples include motion of a pendant group, the chain ends, particular backbone atoms, or motion in the vicinity of crystal defects. Table 1.1 lists representative secondary relaxations for several polymers [51–59]. Secondary relaxations can usually only be resolved unambiguously from the primary α-process below T_g and therefore are measured in the glassy state, where temperature variations only change the thermal energy but not the structure of the material. For this reason secondary relaxations exhibit an Arrhenius temperature dependence (eqn (1.12)). Activation energies are listed in Table 1.1; E_a is on the order of 10 k_BT (k_B is Boltzmann's constant).

Since below T_g a material is (by definition) out of equilibrium, properties of a glass such as volume, enthalpy, and entropy all decrease toward their equilibrium values at a rate that decreases with the extent of supercooling. This phenomenon, known as physical aging, also causes changes in characteristics of secondary relaxations; moreover, the time evolution of properties of the β-process in glasses reflects the structural aging dynamics. This means that

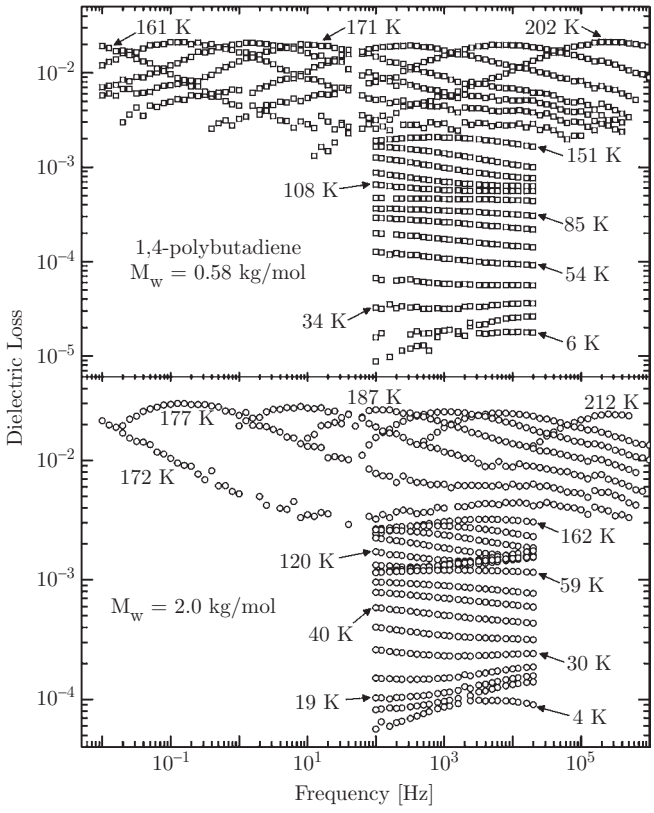

Figure 1.6 Dielectric loss for an oligomeric (upper) and a higher molecular weight (lower) PBD. At the higher temperatures the local segmental peak (α-relaxation) falls within the experimental frequency range, with the Johari–Goldstein secondary process on the high frequency side. At lower temperatures the NCL becomes evident. The measurable span of frequencies is limited at lower temperatures due to the low loss and consequent need to measure using a high-resolution bridge, which has a frequency range of only 2.3 decades. Data from ref. [38].

the time constant for these changes provides a measure of the α-relaxation time, which below T_g is too long for direct measurements. This is illustrated in Figure 1.10, showing α-relaxation times for three materials directly measured above T_g and deduced for the glassy state from changes of the secondary relaxation [60–62].

The JG relaxation is a special type of secondary motion, present in all amorphous or glass-forming materials [63,64]. It is the slowest secondary process and thus can be referred to as the β-relaxation. However, since the JG relaxation is sometimes masked by a strong glass-transition peak, the next higher-frequency secondary process is sometimes inadvertently labeled the β-peak. For small molecules the JG relaxation corresponds to rotation of the entire molecule, although the angle of the reorientation is small, enabling the motion to proceed independently from that of other molecules. The JG relaxation was first discovered in dielectric measurements on rigid molecules [65], whose secondary dynamics cannot involve intramolecular degrees of freedom; all atoms must participate in the process. For polymers

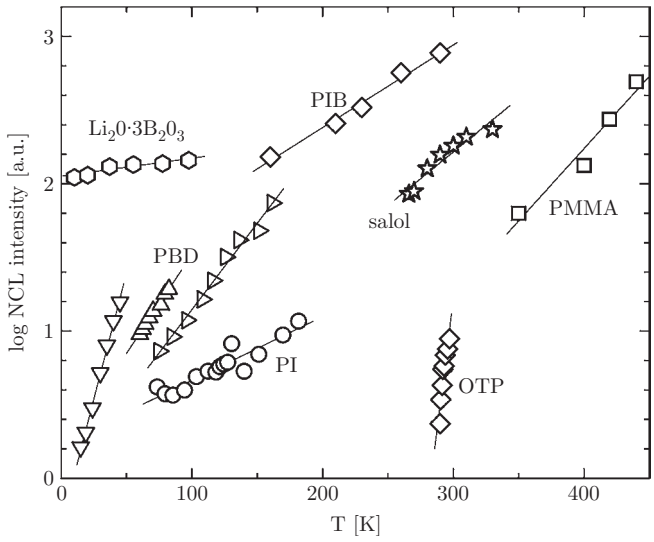

Figure 1.7 Temperature variation of the nearly constant loss in the depolarized light scattering susceptibility of PIB (diamonds, [39]) and PMMA (squares, [40]) and in the dielectric loss of PI (circles, [37]) and PBD (triangles, $M_w = 560$ kg/mol, [28]; inverted triangles, $M_w = 2.0$ kg/mol [38]; right triangles, $M_w = 0.58$ kg/mol [38]). For comparison conductivity of an alkali triborate glass (hexagons [41]) and optical Kerr effect intensities for *o*-terphenyl (pentagons) and phenyl salicylate (stars) [46] in the NCL regime are also shown. Lines are linear fits to the semilogarithmic plots.

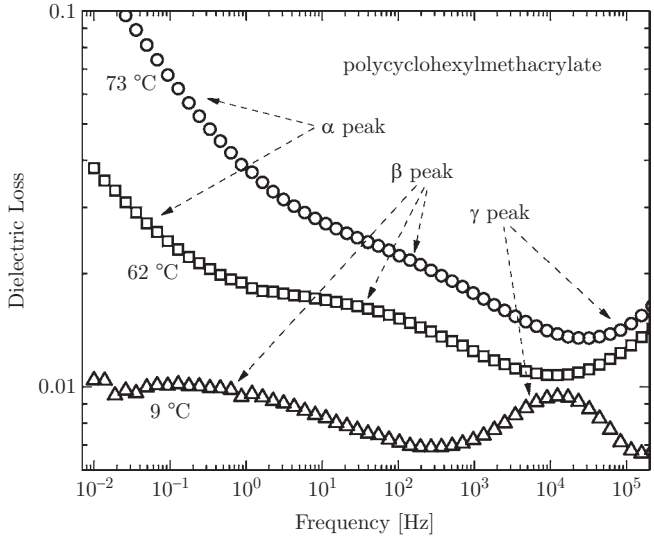

Figure 1.8 Dielectric loss measured for PCHMA [50] at temperatures for which the weak β-peak falls in the measured range of frequencies. The high-frequency side of the strong α-peak appears at higher temperatures. The γ-peak can be seen at frequencies beyond $\sim 10^4$ Hz.

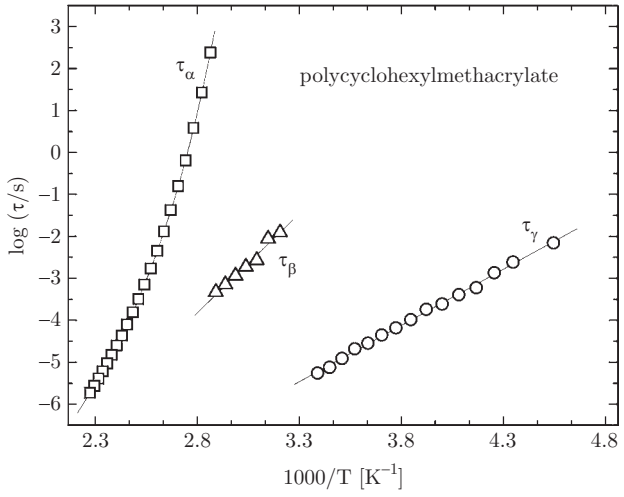

Figure 1.9 Relaxation times of PCHMA determined from the frequency of the maxima in the dielectric loss for the local segmental and two secondary relaxations [50]. The respective temperature sensitivities of the τ increase with increasing timescale of process, becoming non-Arrhenius for the segmental dynamics.

the dynamics of the JG process can be more complicated, but nevertheless a JG relaxation is usually present as the slowest secondary relaxation and one involving the entire repeat unit, not only pendant groups or specific moieties. As an example of a JG relaxation in a polymer, multidimensional NMR experiments on PMMA reveal that the β-relaxation involves 180° flips of the pendant carboxyl group; however, these are coupled to restricted rocking motion of the chain backbone in order to avoid steric interference from other segments (Figure 1.11) [66,67]. The amplitude of this rocking motion increases with temperature, eventually becoming the conformational transitions of the backbone that underlie the segmental dynamics and T_g.

Table 1.1 Non JG secondary relaxations in selected polymers.

polymer	motion	E_a (kJ/mol)	ref.
polyethylmethacrylate	pendant alkyl group motion	7.1	51
polycarbonate	carbonate motion	26	52
	phenyl torsional motion	48	
epoxy polymer	epoxide end group motion	28	53
polyvinyl carbazole	polar side group motion	29	54
nylon	methylene segments rotation	31	55
polystyrene	phenyl group rotation	38	56
styrene–acrylonitrile copolymer	cyano group motion	39	57
polycyclohexylmethacrylate	cyclohexyl flipping	45	58
polyoxymethylene	backbone twisting about crystal defects	80	59

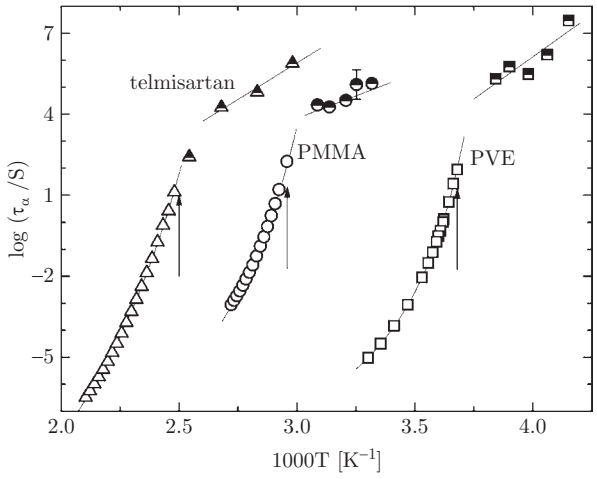

Figure 1.10 α-relaxation times measured above T_g (open symbols) and the values of τ_α deduced from the kinetics of changes in the secondary relaxation due to physical aging (half-filled symbols) for the pharmaceutical telmisartan (triangles) [60], polymethylmethacrylate (circles) [61], and polyvinylethylene (squares) [62]. The departures from Arrhenius behavior above T_g (indicated by the arrows) are absent in the glassy state.

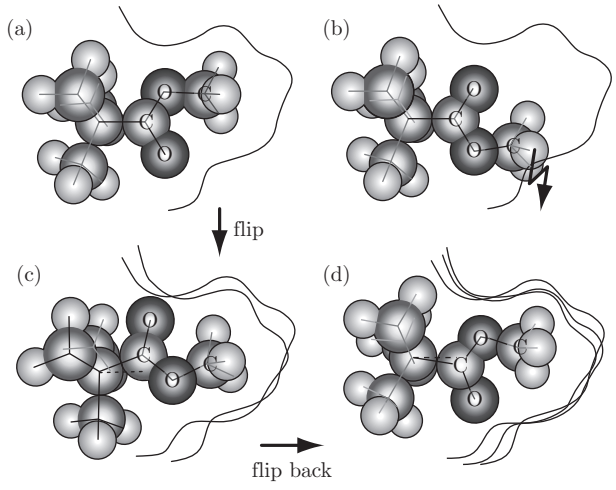

Figure 1.11 Depiction of the motion of the side group in PMMA (a) Initial orientation of the pendant group. (b) Rotation of side-group without backbone motion is sterically hindered by neighboring segments. (c) Twisting about backbone allows the side group to be accommodated by the local empty space; this in turn causes some readjustment of neighboring segments. (d) Counterrotation of the side group returns it approximately to its original orientation but with some alterations due to the changes in the orientations of the backbone and the neighboring segments. [66] (*reproduced with permission*)

Thus, the secondary relaxation in PMMA detected mainly as a side-group motion involves all the atoms and is therefore a JG process.

At higher temperatures and longer times JG relaxations evolve into the primary structural process [68], and for this reason the properties of JG relaxations are correlated with those of the segmental dynamics. The JG relaxation mimics [69] or even serves as the precursor [70] to the glass transition. Nuclear magnetic resonance (NMR) is the most unambiguous method to distinguish whether a secondary process is a JG motion, although this can sometimes be inferred from the greater sensitivity to pressure or volume changes in comparison to motions involving only a portion of the molecule or repeat unit. The properties of JG relaxations are considered in more detail in Chapter 2 dealing with the segmental dynamics of polymers.

1.2.4 Glass transition

The glass transition refers to structural relaxation occurring in the liquid as it vitrifies. T_g is operationally defined as the pressure-dependent temperature at which the local segmental dynamics of polymers (or correspondingly, the reorientation of small molecules or the translation of colloidal particles) transpires on a timescale significantly longer than the experimental time.[12] The local and intermediate range structural order of polymers, as revealed by X-ray and neutron diffraction, changes negligibly as the material is taken from the melt to the glassy state; it is for this reason that amorphous polymer glasses can be regarded as "frozen" liquids. Segmental relaxation of polymers involves skeletal bond conformational transitions, with motion over large length scales avoided by cooperative rotations of neighboring units along the chain (intramolecular cooperativity) [71,72].

Although structural relaxation *per se* is not unique to polymers, interference from crystallization is less of a problem with polymers, as alluded to above, since crystallization is often slow (or even non-existent in the case of copolymers or atactic homopolymers, which have non-uniform repeat units). Molecular liquids have to be quenched to avoid crystallization; hence, the term "supercooled" for amorphous liquids below their melting temperature. This facile vitrification makes polymers well suited for the study of the glass transition, which is a major unsolved problem of condensed-matter physics.

The glass transition is a property of polymers, along with their strength and modulus, that is influenced by the concentration of chain ends [73–75]. If the molecular weight, M, is very high, the concentration of chain ends is negligible and molecular weight effects are absent. The value of M necessary to attain this high-polymer limiting behavior depends on the material. A general rule of thumb is that chain ends exert a measurable effect only for M below *ca.* 10^5 g/mol. However, especially flexible chains, such as those with an oxygen atom in the backbone, retain an insensitivity to molecular weight down to much shorter chain lengths. Note that the high-polymer limiting behavior refers only to the effect of chain ends, but not to chain length *per se*. The slow dynamics of polymers such as the viscosity and frequency range of the rubbery plateau depend non-linearly on M, but this is a size effect and not due to any dependence on the chain-end concentration.

There have been many attempts to model the effect of M on T_g, primarily by invoking an addition from the chain ends to the free volume or configurational entropy. Simulations show that the chain ends are associated with an excess volume compared to the inner chain segments (Figure 1.12 [76]). The difficulty is that the control parameter (density, thermal

[12] This timescale can be estimated as the ratio of T_g to the rate at which temperature is varied.

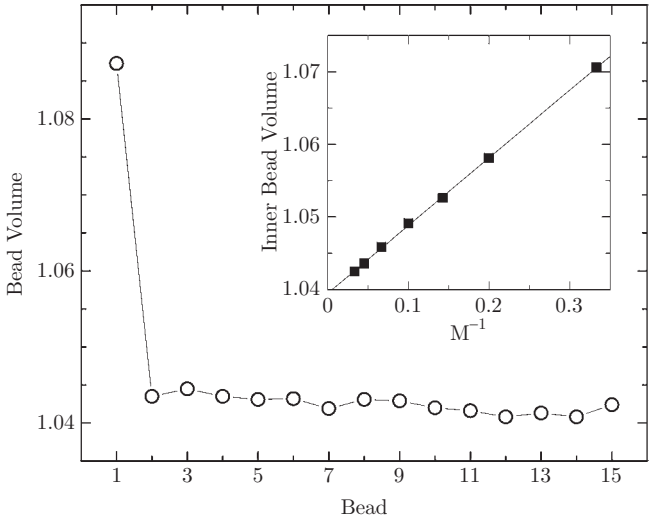

Figure 1.12 Average volume (both occupied and free) per repeat unit as a function of the position of the bead along the polymer chain. The occupied volume of a bead equals unity. The inset shows the variation of the average volume of an inner bead with inverse of the degree of polymerization. The line is the linear fit. Data from ref. [76].

energy, configurational entropy) underlying the segmental dynamics and thus T_g remains an open question, although much progress has been made (see Chapter 2). An early effort due to Fox and Flory [77] assumed that T_g corresponds to a state of constant free volume, leading to an expression for the variation of T_g with the number average molecular weight, M_n, of linear polymers

$$T_g = T_{g,\infty} - k_{FF}/M_n \tag{1.16}$$

where M_n is the mean

$$M_n = \frac{\int_0^\infty \hat{n}\,(M) M dM}{\int_0^\infty \hat{n}\,(M) dM} \tag{1.17}$$

$\hat{n}$ is the number of chains of weight M. In eqn (1.16) $T_{g,\infty}$ is the glass-transition temperature in the absence of chain ends and k_{FF} is a material constant whose value depends on the identity of the end groups [78,79]. An empirical expression more accurate for low molecular weights is [80]

$$T_g^{-1} = T_{g,\infty}^{-1} + K_{UK}/M_n \tag{1.18}$$

where the constant k_{UK} serves the same function as k_{FF}. This equation is seen in Figure 1.13 [81] to describe the T_g of various polystyrenes, including mixtures with linear or ring PS. Alternative expressions not wedded to free volume ideas have been derived [82,83], but other than possibly offering insights into the phenomenon, these have no advantage in describing experimental $T_g(M_n)$ data for linear polymers. Equation (1.16) has been applied to star-branched polymers by multiplying the last term by the junction functionality [83] and to dendrimers by accounting for the generation number [84]. An implication from studies of branched polymers is that the concentration of chain ends governs the glass-transition temperature. However, this is at odds

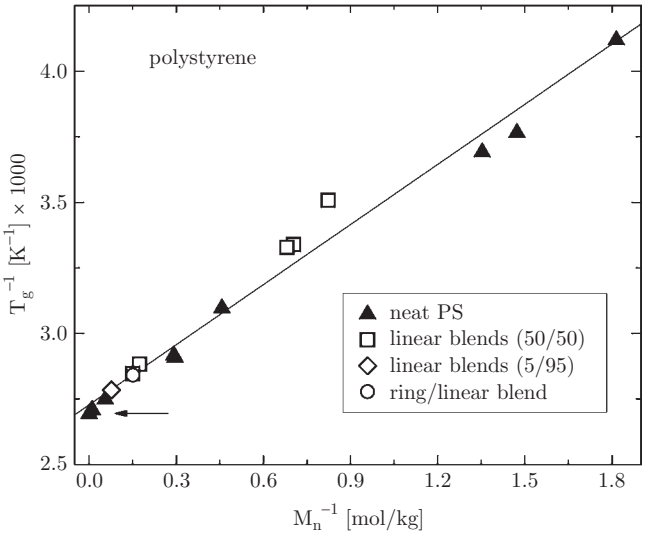

Figure 1.13 Molecular weight dependence of the glass-transition temperature of linear PS plotted in the form of eqn (1.18) for the neat polymer, its blends with 5 and 50% by weight of low M_n (= 739 g/mol) linear PS, and blends with 50% cyclic PS (M_n = 4.4 kg/mol). For the latter 100 kg/mol was used in calculating M_n of the blend, since the ring structure has no chain ends. The arrow indicates the T_g measured for this cyclic PS. Data from ref. [81].

with the invariance of T_g to the degree of branching for PBD 4-, 8- and 12-arm stars, in which T_g depends only on M_n [85]. It may be that in highly branched architectures the freedom conferred by chain ends is countervailed by the constraining effect of the junction points. Other properties are also sensitive to chain ends. For example, since chain ends are not load bearing, they reduce the modulus and strength of a rubber network. Such properties can be described generally by an equation having the form of eqn (1.16).[13]

Since T_g is defined as the temperature at which the material response (i.e. the local segmental dynamics) becomes significantly slower than the experimental measurement rate (Deborah number » 1), the glass transition is rate dependent. This means rapidly strained rubber can behave as a glass; that is, the rubbery state may not persist at high strain rates. As discussed in Chapter 2, strain-induced glass transitions in rubber underlie some applications of elastomers. (The other phase change induced by the deformation of rubber, strain-induced crystallization, can also be affected by strain rate; for example, strain crystallization of natural rubber is curtailed at higher strain rates [86–88])

In addition to the static length scales referred to above, the glass transition is associated with a dynamic length scale reflecting the heterogeneous nature of the reorientational motions. This length scale can be defined as a correlation length, or distance over which the segmental dynamics (or reorientation of small molecules) are mutually correlated. Entropy models of the glass transition embody a related concept, the minimum distance for segmental

[13] Flory [73,74] proposed an equation of this form for the effect of molecular weight on the tensile strength of rubber. Ironically, he applied the analysis to data for strain-crystallizing materials, which complicates an interpretation in terms of the chain-end concentration.

motions to transpire without being accommodated by motion of other segments; this leads to the idea of cooperatively rearranging regions [89,90]. The length scale of the segmental dynamics grows as T_g is approached, becoming macroscopic in the glassy state (Section 2.3.2). Experimental results indicate this length scale in molecular liquids and polymers to be a few nm for temperatures not too far above T_g [91–93]. The corresponding reorientation angle is on the order of 10 degrees [94].

1.2.5 Unentangled chain dynamics

Motions over length scales larger than the correlation length for segmental relaxation transpire at longer times. Those involving only *ca.* 10 backbone bonds may occur as a result of, or even simultaneously with, the local segmental dynamics; that is, the glass transition comprises conformational transitions that permit relaxation to proceed beyond the locally relaxing segments themselves. These longer modes are designated "sub-Rouse modes" [95,96] to convey that the segments involved, while larger than the couple of conformers involved in local segmental relaxation, contain fewer repeat units than the shortest of the Gaussian submolecules described by the Rouse model. The sub-Rouse motion is not evident in measurements probing only the local modes, such as most dielectric relaxation and quasi-elastic photon and neutron-scattering spectroscopies. However, since almost all modes contribute to the stress, the sub-Rouse dynamics can be detected in favorable cases by mechanical experiments. To be apparent as a distinct spectral feature, however, requires that the sub-Rouse modes are not subsumed by the intense segmental process.

Polyisobutylene has many unusual properties, including a similar temperature variation of its segmental and Rouse dynamics [97,98], due to the weak T-dependence of the local segmental motions (see Chapter 6). The result is that the two viscoelastic mechanisms are widely separated in time (more so than for most polymers) in typical mechanical measurements, enabling resolution of the sub-Rouse modes. This is illustrated in Figure 1.14 showing the loss tangent ($\tan\delta$, defined as the ratio of the out-of-phase and in-phase components of the dynamic modulus) for PIB at various temperatures [99]. Note that the abscissa is actual frequency; these are not master curves. The unusually broad, structured nature of the peak is ascribed to the prominence of the sub-Rouse modes in PIB.

If a flexible chain has at least 20 to 50 backbone bonds, correlations between bonds are lost, and the dynamics can be described by the Rouse model [100]. The polymer molecule is modeled as a freely jointed chain undergoing random-flight statistics. The end-to-end distribution function $P(r)$ is based on the inverse Langevin function, which can be expressed as a series expansion of the form [101]

$$P(r) \sim \exp\left\{-n_K\left[\frac{3}{2}\left(\frac{r}{n_K l_K}\right)^2 + \frac{9}{20}\left(\frac{r}{n_K l_K}\right)^4 + \frac{99}{350}\left(\frac{r}{n_K l_K}\right)^6 + \ldots\right]\right\} \tag{1.19}$$

where n_K is the number of steps in the random walk and l_K is the step length. For moderate extensions this series can be truncated after the first term to give the Gaussian approximation

$$P(r) = \left(\frac{3}{2\pi n_K l_K^2}\right)^{3/2} \exp\left(-\frac{3r^2}{2n_K l_K^2}\right) \tag{1.20}$$

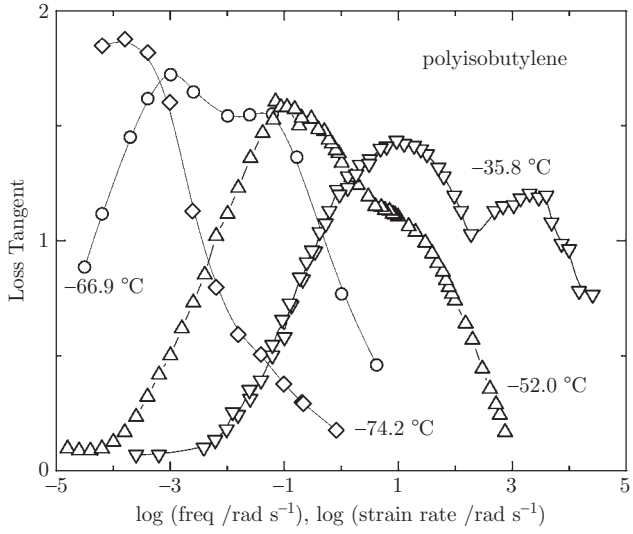

Figure 1.14 Loss tangent of polyisobutylene measured by dynamic mechanical spectroscopy and calculated from the recoverable creep compliance. Note the abscissa is actual frequency; these are not master curves. Data from ref. [99].

The prefactor in eqn (1.20) results from normalization of the distribution function

$$\int_0^\infty P(r) 4\pi r^2 \, dr = 1 \tag{1.21}$$

Gaussian distributions are common because of the statistical property that the arithmetic mean (normalized sum) calculated for any independent random variable approaches a Gaussian distribution, independent of the original distribution of the variable.[14] Deviations from eqn (1.20) are small over the usual range of interest; moreover, the Gaussian approximation is exact for $\langle r^2 \rangle$, since it involves only averages (that is, the Central Limit Theorem applies). The absence of correlations between successive steps leads to a simple relation

$$\langle r^2 \rangle = n_K l_K^2 \tag{1.22}$$

A macromolecule, or a section of it, conforming to eqn (1.20) is called a "Gaussian chain," with n_K the number of backbone bonds of length l_K.

Of course, real chains are not freely jointed but are confined to fixed torsional angles involving conformational states of different energy. The connection to random-flight statistics is made by redefining n_K and l_K of the equivalent "Kuhn" chain in terms of the number, n, and length, l, of actual backbone bonds. There are two equivalences: (i) the fully extended dimension

$$n_K l_K = nl \sin(\theta/2) \tag{1.23}$$

[14] This property, known as the Central Limit Theorem, expresses the fact that a Gaussian distribution maximizes the entropy [102].

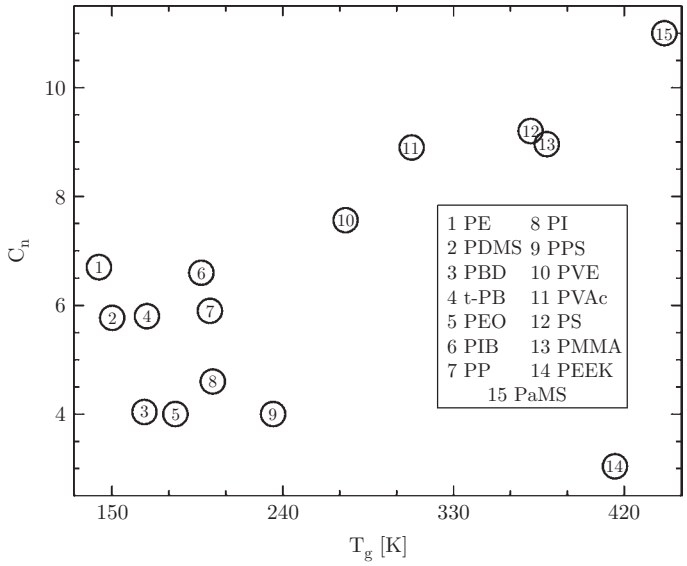

Figure 1.15 Characteristic ratio of various polymers plotted *vs.* their glass-transition temperature. Both properties are affected by the flexibility of the chain. Data from refs. [104 and 103].

where θ is the bond angle ($= 109.5°$ for carbon–carbon single bonds), and (ii) the mean square end-to-end distance

$$\langle r^2 \rangle = C_n n l^2 \tag{1.24}$$

By definition then, l_K is twice the persistence length, l_p. In eqn (1.24) C_n is the characteristic ratio, a measure of chain stiffness. This parameter increases with molecular weight to a constant value at large n, C_∞. Since the glass-transition temperature also increases with stiffness of the polymer backbone, there is a rough correlation between C_∞ and T_g, as illustrated in Figure 1.15 (some of the scatter of these data [103,104] represents differences in the measurement conditions).

The force, f_e, required to maintain a deformation of the chain can be determined from the Helmholtz energy

$$A = E - TS \tag{1.25}$$

where E and S represent the internal energy and entropy, respectively. The thermodynamic relation for an isothermal, isochoric change in chain dimension is [103]

$$f_e = \left.\frac{\partial A}{\partial r}\right|_{T,V} = \left.\frac{dE}{dr}\right|_V - T\left.\frac{dS}{dr}\right|_T \tag{1.26}$$

Using the definition of the entropy[15]

$$S = k_B \ln P(r) \tag{1.27}$$

[15] Equation (1.27) appears at the top of the tombstone marking Ludwig Boltzmann's grave in Vienna, Austria.

eqn (1.20) yields

$$f_e = \left.\frac{dE}{dr}\right|_{T,V} + \frac{3k_BT}{\langle r^2\rangle} r \tag{1.28}$$

in which r represents the distension of the chain from its equilibrium length. If the chain configurations all have the same conformational energy, the elastic force on a chain is purely entropic and directly proportional to the temperature

$$f_e = \frac{3k_BT}{\langle r^2\rangle} r \tag{1.29}$$

This force increases linearly with the end-to-end distance; thus, Gaussian chains can be regarded as entropy springs conforming to Hooke's law. There are two obvious deviations for real chains: The underlying random-walk model cannot describe the finite extensibility of polymer chains, so eqn (1.29) is limited to small or moderate strains. And conformations have different energies, so that the internal energy of a real chain changes with conformation ($\left.\frac{dE}{dr}\right|_T \neq 0$), with experiments indicating this energetic contribution is typically 10–20% of the total strain energy [101]. Further discussion of the elastic properties of chains is deferred to Chapter 4.

In the Rouse model the motion of a chain is resisted by drag from the surroundings due to interactions with neighboring segments. These complex interactions can be approximated by an average friction coefficient ζ, which can be identified with the friction coefficient governing local segmental relaxation. This friction deforms the chain, giving rise to a counter force specified by eqn (1.29). Neglecting inertia (since the chain is immersed in a viscous medium and the frequencies are not too high) the equation of motion is

$$\zeta \frac{dr}{dt} + f_e = 0 \tag{1.30}$$

The solution to eqn (1.30) has the form [100]

$$r = r_0 \cos\left(\frac{p\pi n}{\hat{N}}\right) \exp(-t/\tau_p) \tag{1.31}$$

where $\hat{N}$ is the number of Gaussian submolecules comprising the chain. Thus, the complex chain dynamics are decomposed into a series of independent normal modes, corresponding to $p = 1, 2, 3, \ldots$, with $p = 0$ representing center of mass motion (uniform translation). The amplitude is r_0 and the relaxation time of the pth mode is given by

$$\tau_p = \frac{\langle r^2\rangle \zeta}{12k_BT \sin^2\left(\frac{\pi p}{2n}\right)} \tag{1.32}$$

Emphasizing the dominant contribution from the longer modes ($n \gg p$), the sine is replaced by its argument to yield

$$\tau_p = \frac{\langle r^2\rangle \zeta n^2}{3k_BT\pi^2 p^2} \tag{1.33}$$

Each mode conforms to eqn (1.20) with the shortest mode encompassing one Gaussian submolecule. Equation (1.33) shows that the relaxation time of a Rouse chain varies as n^2. The diffusion coefficient obtained from the Einstein relation

$$D_R = \frac{kT}{\zeta_{chain}} = \frac{kT}{n\zeta} \sim n^{-1} \tag{1.34}$$

varies inversely with chain length, since the friction coefficient for the chain, ζ_{chain}, is the sum over the entire chain of the local friction coefficient of each segment and thus proportional to n. From this description of the motion of the submolecules, the forces on each subchain can be summed to obtain an expression for the modulus

$$G(t) = ck_BT \sum_{p=1}^{n} \exp(-t/\tau_p) \tag{1.35}$$

for c chains per unit volume. This equation has the same form as the modulus expression for n parallel Maxwell elements (a spring in series with a dashpot). However, it is important to recognize that the form of eqn (1.35) comes from a mode analysis. Any smooth closed curve can be represented by a Fourier sum; the Gaussian submolecules are an artifice used to deduce the response of a chain to a perturbation. The additivity of the contributions from each mode does not imply, for example, that different components of stress are additive in any general way. This topic is examined in more detail in Chapter 5.

Originally, the Rouse model was derived for chains moving independently in dilute solution. Since no assumptions are made about the nature of the solvent, Bueche [105] pointed out that such a model can be applied to neat polymers, with neighboring segments serving the role of the solvent. The only restriction is that the effect of the surrounding chains is limited to influencing the magnitude of the friction coefficient, ζ; that is, there is no entanglement effect. Additionally, the absence of excluded volume and hydrodynamic interactions in the Rouse model (see Chapter 3), both of which are important for the dynamics of polymers in dilute solution, enhances the applicability of the Rouse model to concentrated solutions and melts of low molecular weight polymers.

The dynamic moduli corresponding to the Rouse relaxation modulus in eqn (1.35)) are given by the Fourier transforms

$$G'(\omega) = \omega \int_0^\infty G(t) \sin \omega t dt \tag{1.36}$$

$$= ck_BT \sum_{p=1}^{\infty} \frac{\omega^2\tau_p^2}{1+\omega^2\tau_p^2} \tag{1.37}$$

for the storage modulus and

$$G''(\omega) = \omega \int_0^\infty G(t) \cos \omega t dt \tag{1.38}$$

$$= ck_BT \sum_{p=1}^{\infty} \frac{\omega\tau_p}{1+\omega^2\tau_p^2} \tag{1.39}$$

for the loss modulus. At low enough frequencies the limiting behavior $G'(\omega) \sim \omega^2$ and $G''(\omega) \sim \omega$ is obtained. Over an intermediate frequency range, prior to very short times where the model breaks down, the prediction is that the modulus varies according to $\omega^{1/2}$. The quadratic dependence on molecular weight in eqn (1.33) is borne out approximately for the longest ($p = 1$) Rouse mode by experiments on unentangled polymers (see Chapter 3). Although the model

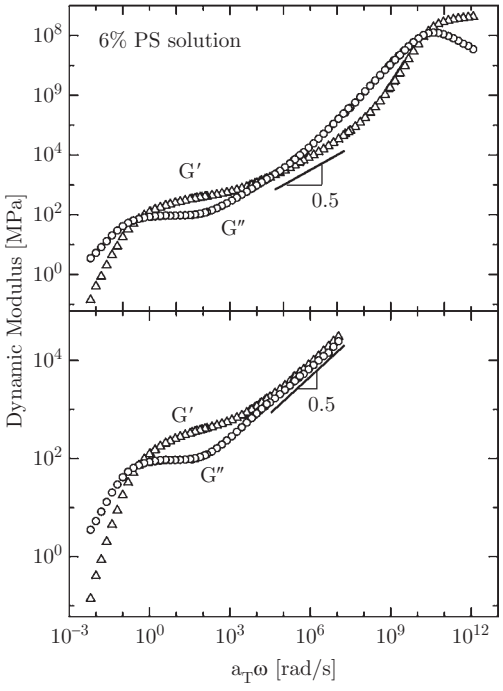

Figure 1.16. Dynamic storage and loss modulus *vs* reduced frequency for 6% PS (5.48×10^6 D) in diethyl phthalate solutions. The lower curve is after subtraction of the solvent and local segmental contributions to the dynamic moduli. Data from ref. [106].

does not address the effect of entanglements, the Rouse description remains valid for high molecular weight melts at times before the onset of entanglements effects. This is illustrated in Figure 1.16 [106], wherein the ω^2 behavior in eqn (1.37) is observed for frequencies higher than the entanglement plateau in measurements on a concentrated solution of high molecular polystyrene. This power-law behavior continues well into the transition zone in this example because the contribution from the segmental dynamics has been subtracted from the spectrum [106]. With its basis in Gaussian chain statistics, the Rouse model applies to flexible polymers. There are indications that stiff chains, having persistence lengths larger than the distance between entanglements, lack Rouse motion at any timescale [107,108].

The Rouse model describes the response of an ensemble of chains. Quantities defined by equations such as (1.20) describe a spherical probability distribution because the conformations are pre-averaged over all chain orientation. However, the shape of chain molecules (the length, width, and depth of the chain conformation), or of Gaussian paths in general, is not spherical. The segment distribution is more extended along one axis than the other two, giving rise to a shape like an oval bar of soap; that is, close to prolate but with unequal minor axes [109–111]. With increasing molecular weight, the departure of the chains from spherical symmetry is reduced; nevertheless, the high molecular weight limiting shape is still highly non-spherical. This asymmetry can be expressed as the ratios of the radius of gyration measured along each of the three principle axes, which for linear chains (the most asymmetric polymers) equal 1:1.7:3.6 [112–114]. It should be emphasized that this non-spherical segment

distribution describes the average configuration of a chain molecule; in the absence of orientation the ensemble average values are $\langle R_x^2 \rangle = \langle R_y^2 \rangle = \langle R_z^2 \rangle = \frac{1}{3}\langle R_g^2 \rangle$. The elongated shape of polymer chains influences events transpiring over timescales smaller than the terminal relaxation time. This is the reason why during viscous flow the stress field can orient chains without causing their stretching.

1.2.6 Dynamics of high polymers

Most applications of polymeric materials employ high molecular weight polymers, which have rheological properties distinctly different from unentangled chains. Given its practical importance, the flow of polymeric materials has been an area of intense research over the past half-century. The uncrossablity of polymer chains leads to the idea of topological constraints to explain the rheology. The effects of these constraints are brought out clearly in plots of various dynamic properties as a function of molecular weight. However, the chains of a given material are not all the same length, requiring the use of averages to describe the distribution of molecular weights. These include the arithmetic mean defined in eqn (1.17), the weight average molecular weight:

$$M_w = \frac{\int_0^\infty \hat{n}\,(M) M^2 dM}{\int_0^\infty \hat{n}\,(M) M dM} \tag{1.40}$$

and the so-call z-average:

$$M_z = \frac{\int_0^\infty \hat{n}\,(M) M^3 dM}{\int_0^\infty \hat{n}\,(M) M^2 dM} \tag{1.41}$$

Other measures of molecular weight include the peak value, M_p, which corresponds to the maximum in the distribution, and M_v, determined from the intrinsic viscosity, $[\eta]$, using the Mark–Houwink relation [115]

$$[\eta] = \hat{K} M_v^{\hat{a}} \tag{1.42}$$

where $\hat{K}$ and $\hat{a}$ are empirical, polymer-specific parameters. The size of the molecular can also be expressed in terms of the degree of polymerization, N, which is the corresponding M divided by the molecular weight of the repeat unit, m_0. The breadth of the chain length distribution is described by the polydispersity index

$$P_i = M_w / M_n \tag{1.43}$$

This index is related to the variance, σ_V^2, or averaged squared difference of the chain lengths from their mean, according to

$$\sigma_V^2 = (P_i - 1) M_n^2 \tag{1.44}$$

The different M averages are denoted in Figure 1.17 showing the molecular weight distribution of a styrene–butadiene copolymer, polymerized using an organolithium initiator. This is an example of an anionic "living" polymerization [116], which can yield fairly monodisperse materials, having a molecular weight distribution approaching the Poisson distribution, for which

$$P_i = m_0 / M_n \tag{1.45}$$

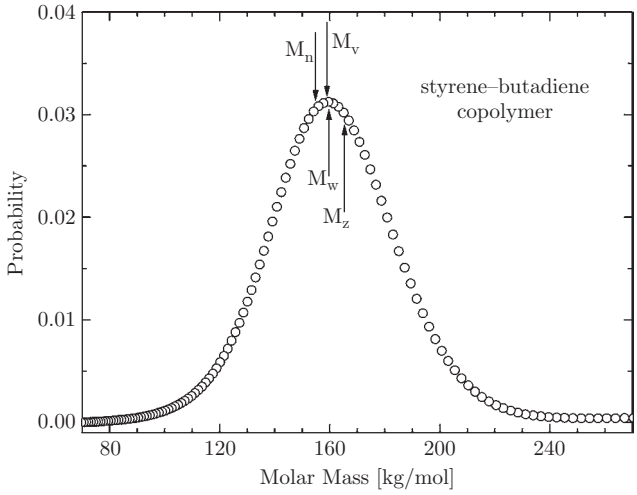

Figure 1.17 Molecular weight distribution measured by gel permeation chromatography for an SBR (19.5% styrene) obtained by anionic polymerization using an organolithium initiator. The polydispersity index = 1.03; for a Poisson distribution with this same M_n, $P = 1.004$. (*Courtesy of Terry Hogan of the Bridgestone Americas Center for Research and Technology.*)

where m_0 is the repeat unit molecular weight. Monodisperse polymers are required for fundamental studies because of the non-linear dependence of the rheological properties on molecular weight, as described below.

For polydisperse polymers the rheological properties are generally expected to be a function of the weight average molecular weight [117]; thus, the zero-shear viscosity, η_0, the length of the rubbery plateau in the relaxation and storage moduli, and the terminal relaxation time, τ_η, are assumed to be proportional to M_w^d where the exponent $d \geq 1$. However, the actual relationship is more complicated. For example, it has been found for model blends of monodisperse polymers that using M_w significantly overestimates the melt viscosity [118–120].

When the chains are long enough to entangle, a rubbery plateau becomes evident in the dynamic mechanical spectra (Figure 1.1). This plateau behavior continues until the chains have sufficient time to relax via disentanglement, with the reciprocal of the characteristic frequency of this relaxation defining a terminal relaxation time, τ_η. Since lateral motions are suppressed, the chain follows an anisotropic path along its own coarse-grained contour [121]. The Doi–Edwards tube model [122] provides a theoretical framework for this reptation concept and, with various refinements, has become predominant in the field of polymer rheology. The tube model has two species-dependent parameters, the Rouse friction coefficient, ζ, and a parameter characterizing the concentration of entanglements.

The snake-like motion of the chain is Brownian diffusion in a tube, with the equation for Fickian diffusion

$$\tau = \langle x^2 \rangle / D \tag{1.46}$$

used to obtain predictions for the chain-length dependences of the terminal relaxation time (i.e. the time for a chain to escape its tube) and the self-diffusion constant. With x ($\propto n$) representing the contour length of the chain and D_R ($\propto n^{-1}$) used for the diffusion coefficient

(the chain dynamics inside the tube are unaffected by entanglements), the terminal relaxation time is predicted to vary as $\tau_\eta \sim n^3 \sim M_w^3$. The zero-shear rate viscosity is the integral of the stress relaxation modulus,

$$\eta_0 = \int_0^\infty G(t)\,dt = \int_0^\infty tG(t)\,d\,\ln t \tag{1.47}$$

so η_0 has the same cubic dependence on molecular weight. The macroscopic diffusion coefficient for entangled chains is also obtained from eqn (1.46). During a time on the order of τ_η, the chain travels a distance roughly equal to its size, so $\langle x^2 \rangle$ (now the macroscopic diffusion distance not the length of the tube) is proportional to n (eqn (1.24)) and thus $D_{rep} \sim n^{-2} \sim M_w^{-2}$ according to the tube model.

There exists an enormous amount of experimental data allowing these tube model predictions to be tested [123–126]. The overriding conclusion is that the actual dependence is stronger than predicted for the relaxation time and viscosity; experimentally $\tau_\eta \sim \eta_0 \sim n^{3.4–3.7}$, meaning the tube model underestimates the effect of chain length on the terminal dynamics. In Figure 1.18 viscosity data [127–130] are shown for three polymers having molecular weights exceeding one million g/mol. Since these polymers, amorphous polyethylene (PE), PBD, and PI, have small entanglement molecular weights, M_e, these materials attain exceptional degrees

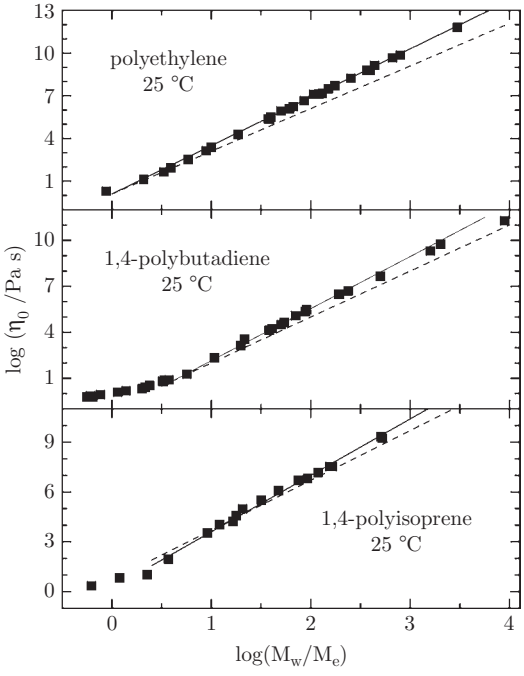

Figure 1.18 Zero-shear rate viscosities of polyethylene [127,128], 1,4-polybutadiene [129], and 1,4-polyisoprene [130] as a function of the number of entanglements per chain, using $M_e = 1.20$, 1.85, and 6.19 kg/mol for PE, PBD, and PI respectively. η_0 have been shifted to 25 °C using reported shift factors. The solid line, conforming well to the data, has a slope of 3.4 and the dashed line has a slope equal to 3.0, representing the tube-model prediction.

Table 1.2 Molecular weight dependence of diffusion coefficients ($D \sim M^{-U}$) for entangled polymers [ref. 126 and references therein].

	U	
polymer	self-diffusion	tracer diffusion
polystyrene	2.3 ±0.3	2.0 ±0.1
polyethylene	2.2 ±0.2	2.0 ±0.1
polydimethylsiloxane	2.2 ±0.2	—
polyethylene oxide	2.2 ±0.2	—
1,4-polybutadiene	> 2.0	—
1,4-polyisoprene	—	1.9

of chain entanglement; nevertheless, the molecular weight dependence in all cases is significantly stronger then M^3. The variation of self-diffusion coefficients with molecular weight is also at odds with the tube model. Experimentally $D_{self} \sim n^{-2.2 \pm 0.2}$ (Table 1.2), rather than a quadratic dependence.

The usual explanation for the deviations in molecular weight dependences is that other relaxation mechanisms contribute to the entangled chain dynamics, thereby diminishing the topological confinements. The tube itself, being composed of neighboring chains, relaxes over the timescale of the reptation time, leading to: *constraint release*, movement of chain segments comprising the tube out of the path of the given chain, and *contour length fluctuations*, movement of the ends of the tube. There is a belief that at very high M "pure reptation" might be obtained as the other relaxation mechanisms become inoperative. For example, if the data in Figure 1.18 are replotted using $M_w^3\eta_0$ as the ordinate variable, there is arguably a suggestion of some flattening of the curve for the higher M_w, consistent with approach to a cubic power dependence on M_w. From the experimental side it is not easy to obtain measurements on polymers with a thousand or more entanglements per chain, since the relaxation times are so long. If solvents are employed for sample preparation, it is difficult to ensure that an equilibrium degree of entanglement has been attained in the material prior to testing. And to reduce the duration of the measurements, temperatures must be used at which chemical degradation can be significant.

Moreover, it is not clear how pure reptation can ever be achieved with homogeneous melts, since the relaxation times of the entangled chain and of the chains comprising the tube scale equivalently with molecular weight. However, for diffusion of probe chains dissolved in a matrix of higher M polymer, constraint release and contour length fluctuations of the tube are suppressed over the timescale of the probe chain motion. This implies that the diffusion coefficient of probe chains should exhibit the expected n^{-2} behavior, an expectation borne out by experimental data (Table 1.2).

1.3 Fluctuations and linear response theory

Small fluctuations of properties from their average value, arising from thermally driven motion of the constituent molecules, are inherent to materials. These microscopic motions allow a system to transition from a metastable state to the thermodynamically stable one. This effect is apparent during the inflation of rubber balloons. Figure 1.19 shows the

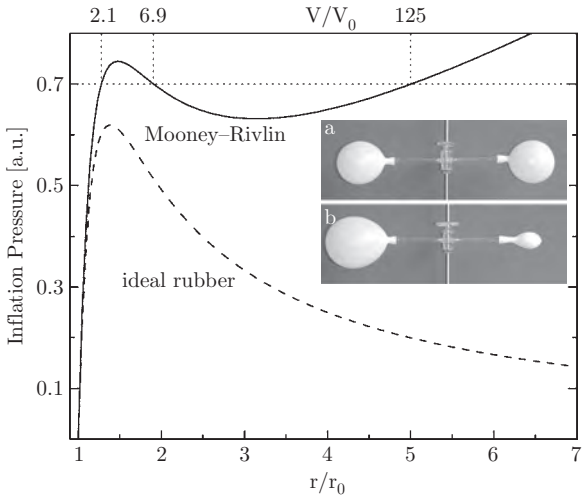

Figure 1.19 Pressure during isothermal inflation of a thin spherical elastomer calculated assuming linear behavior (eqn (1.29); dashed line) and a more realistic response (eqn. (4.9) of Chapter 4; solid line). The intersection with the horizontal dotted line denotes three possible equilibrium states for $P = 0.7$. The photographs (*courtesy of Peter Strehlow of the Technische Universität Berlin*) depict two identical balloons inflated to the same pressure. (a) Initially their volumes are equal. (b) After opening a valve to allow interchange of the contained air, there is a spontaneous change to unequal volumes, with the final pressure unchanged.

pressure–volume curve of a balloon (dashed line) calculated using the ideal chain model (eqn (1.29)), which is valid only for small strains. Introducing non-linearity (see Chapter 4) into the elastic response gives the inflation behavior observed in real balloons (solid curve). As the volume increases there is a steep rise in pressure, followed by a decreasing P until very high volumes are attained (this non-monotonic response is apparent when using one's lungs to inflate a balloon). Note that the variation of the force on the rubber with inflation volume is a combined function of LaPlace's law,[16] the diminishing cross-sectional area, and the form of the force–extension relation for the biaxially strained elastomer. Beyond the maximum in P, the expansion is unstable and non-uniform.

To see the effect of equilibrium fluctuations on inflated balloons, consider the two identical balloons in Figure 1.19, initially at the same pressure P ($= 0.7$ in arbitrary units) and volume ($V/V_0 = 6.9$) but separated by a closed tube [131]. Upon opening a valve in the connecting tube, the pressures will remain the same and equal for the balloons; however, this pressure balance exists for three different inflation volumes. For moderate pressures and depending on the details of the elastic properties of the material, the balloons spontaneously transition to smaller and larger volumes respectively (e.g., $V/V_0 = 2.1$ and 125). This behavior, depicted in the photographs in the inset to Figure 1.19, is non-intuitive but well understood (and possible

[16] According to LaPlace's law, the surface tension in the balloon at fixed inflation pressure is proportional to its radius of curvature.

only for inflation strains sufficient for deviations from eqn (1.29) [132,133]). The question is, how did the balloon ending at the lower $V/V_0 = 2.1$ in Figure 19 traverse the intermediate volumes associated with higher pressures? The answer is by fluctuations in the pressure. Analogous to chemical reactants overcoming an activation barrier to form lower-energy products, the final inflation conditions of the two balloons can be achieved because of random fluctuations inherent to an equilibrium system.

The same fluctuations prevailing at equilibrium enable a material to return to equilibrium following a small external perturbation. Fluctuation-dissipation theory (FDT) relates the fluctuations to how the system responds to (dissipates) external forces. According to FDT, if the material is driven not too far from equilibrium, it is sufficient to know the behavior of the dissipating and perturbing systems in the absence of any coupling in order to predict their interaction; that is, decay of a spontaneous thermal fluctuation cannot be distinguished from decay of fluctuations induced by small external forces. The fluctuating properties can be described through time correlation functions, defined as

$$C(t) = \langle A(0) \cdot B(t) \rangle \tag{1.48}$$

where $A(t)$ and $B(t)$ are microscopic quantities whose values depend on the coordinates and momenta of the constituent molecules. An autocorrelation function quantifies the correlation of a property with its own prior value

$$C(t) = \langle A(0) \cdot A(t) \rangle \tag{1.49}$$

The ensemble average varies over time due to the stochastic fluctuations. Since the system is stationary at equilibrium, average quantities are time independent and the initial time is artificial; that is, $\langle A(0)A(t) \rangle = \langle A(u)A(t+u) \rangle$ and $\langle A(0)[dA(t)/dt] \rangle = d\langle A(u)A(t+u) \rangle dt$, with t specifying the duration between successive evaluations of A. For an ergodic system this average over the system is equivalent to the time average

$$C(t) = \lim_{\hat{t} \to \infty} \hat{t}^{-1} \int_0^{\hat{t}} A(u)A(t+u)du \tag{1.50}$$

Normalization of $A(t)$ by its initial value, $\langle A^2 \rangle$, and subtraction of the long-time asymptotic, uncorrelated value, $\langle A \rangle^2$, makes $C(t)$ equal unity initially and zero eventually. $C(t)$ is calculated by solving the equations of motion describing the coordinates and momenta over time, and averaging over all phase space. A model with suitable assumptions is used to simplify this general N-body problem.

FDT connects the fluctuations described by $C(t)$ to a susceptibility characterizing fluctuations induced experimentally (the latter more accessible than spontaneous fluctuations). The initial statement of FDT was the Nyquist theorem [134] describing Johnson electrical noise [135]. This is the white noise in a conductor due to thermal motion of the electrons, manifested as voltage fluctuations having a mean square potential proportional to the resistance. The resistance, or impedance, is the response measured when an external voltage is applied. More generally experiments yield a susceptibility function describing the change of an observable induced by an infinitesimal perturbation ς

$$\chi(t) = \lim_{\varsigma \to 0} \frac{\langle A(t) \rangle_\varsigma \langle A \rangle_0}{\varsigma} \tag{1.51}$$

According to FDT $\chi(t)$ is related to $C(t)$ as [136,137],

$$\chi(t) = \frac{C(t)}{k_B T} \tag{1.52}$$

The temperature factor accounts for the fact that fluctuations are thermally driven. The Fourier transform of $C(t)$ yields the spectral density and therefore the dynamic susceptibility, $\chi(\omega)$. An example of the FDT is the Einstein relation, eqn (1.34), relating the Brownian motion of particles to viscous dissipation. $A(t)$ and $B(t)$ in eqns (1.48) and (1.49) depend of course on the nature of the experiment. In a transient mechanical experiment, A represents the local stress and the stress relaxation modulus is

$$G(t) = \frac{V}{k_B T} C(t) \tag{1.53}$$

In a dielectric experiment the time-dependent fluctuations of the polarization are measured and $A(t)$ is identified with electric dipoles on the molecules or segments. In most polymers this dipole moment is oriented transverse to the chain, so that the dielectric experiment probes the local segmental dynamics. For those few polymers having a dipole moment parallel to the backbone (which means their repeat unit structure lacks a symmetric center), dielectric relaxation measures the autocorrelation of the chain's end-to-end vector. Note that although the dipoles orient in the presence of the applied field, the interaction energy is much less than the available thermal energy; this is a characteristic of the linear response regime.

Quasi-elastic scattering techniques can be used to probe fluctuations of the polarizability (light scattering), density (X-rays), and nuclei (neutrons) of the molecules, where in favorable cases the motion can be identified with a particular axis or moiety in the molecule. The scattered intensity varies with the wave vector, $q = \frac{4\pi}{\lambda} \sin(\theta/2)$, where θ is the scattering angle and λ the wavelength. This angle dependence of the intensity means that scattering experiments yield information about the variation of the molecular motions with length scale, information not available from mechanical or dielectric relaxation spectroscopies. The characteristic length scales must be on the order of the wavelength, which distinguishes light, X-ray, and neutron measurements. Scattering experiments are able to probe correlations between different particles. For example, the intermediate scattering function, $F(q,t)$, measured by quasi-elastic X-ray and neutron experiments, is related to the correlation function according to

$$C(r,t) = C_s(r,t) + C_c(r,t) = \frac{1}{8\pi^3} \int \exp(iqr) F(q,t) dq \tag{1.54}$$

in which $C_s(r,t)$ and $C_c(r,t)$ described the self- and cross-correlations respectively. Other examples of experimentally accessible correlation functions are for nuclear magnetic dipoles, probed by NMR measurements, and chromophores attached to polymers chains, responsible for fluorescence decay and holographic grating techniques.

Two restrictions in the application of FDT are that the perturbed system begins in a state of equilibrium and that the external perturbation does not drive the material beyond values of $A(t)$ attainable by equilibrium fluctuations. The latter is the linear response requirement that determines the amplitude limit for the perturbation. For an initially non-equilibrium system the correlation and response functions deviate from FDT; nevertheless, the theory can still be useful. For example, in some situations the departure from equilibrium can be quantified by defining an effective temperature in analogy with eqn (1.52) [138–140]

$$T_f = k_B^{-1}\left[\frac{C(t)}{\chi(t)}\right] \tag{1.55}$$

The quantity in brackets is called the fluctuation-dissipation ratio, which approaches unity close to equilibrium. T_f is the temperature at which the observed non-equilibrium properties would have their equilibrium values. For glasses, which are prototypical non-equilibrium materials, T_f is known as the fictive temperature. During physical aging of a glass, the structure moves towards equilibrium and thus T_f approaches the actual temperature.

From the measured susceptibility FDT enables the relevant time correlation function to be obtained. Its interpretation, however, relies on computation of $C(t)$ from a model of the dynamic process probed by the experiment. For the case of reorientational motions, Debye [2] proposed a simple model wherein the liquid molecules change orientation through a series of small angular jumps due to unbalanced torques from the fluctuating surroundings (random "collisions"). The motion is thus a random walk in angular coordinate space, with the time between changes in orientation long compared to the time of a reorientation; i.e. the rotational correlation time is much longer than the correlation time for the angular momentum. Motion of this nature can be described by a diffusion equation whose solution is exponential decay (i.e. the form of a first-order rate equation such as eqn (1.4)). This in turn is the form FDT predicts for the experimental relaxation function. However, there are two obvious cases where the assumptions underlying the Debye model break down. If unbalanced forces are sparse and infrequent, large changes in orientation can occur by free rotation (inertially driven) interrupted by periodic perturbations; such motion cannot be described as a random walk. This situation prevails in low-density fluids, with the relevant $C(t)$ depending on the effect assumed for the perturbations. For example, intermolecular collisions may randomize the instantaneous orientation of the molecule or scramble its angular momentum. This type of motion is not relevant to polymers.

With increasing density in supercooled liquids and polymers, there is a crossover from continuous small-amplitude Brownian motion to discontinuous, large-amplitude hopping as movements become highly correlated – a given segment's change in position or orientation requires motion of its neighbors. The Debye model's mean-field description of a fluctuating environment is inadequate, and measured correlation functions deviate from simple exponential decay. Relaxation in such complex correlated systems often conforms to the Kohlrausch equation (eqn (1.7)). Although it is used as an empirical fitting function, this form can be arrived at in various ways: from models based on free volume [141], hierarchal constraints [142], defect diffusion [143], defect distances [144], random free energy [145], or molecular weight polydispersity [146]; by employing a particular distribution of exponential decay functions [147]; or from specific ideas about cooperativity [148,149]. One approach is to assume that many-body interactions modify the rate constant k in eqn (1.3) during the course of the relaxation according to [148]

$$k(t) = k_0(t/t_0)^{-1/\beta} \tag{1.56}$$

in which t_0 is a constant. When substituted into eqn (1.3), eqn (1.56) gives stretched exponential decay. When many-body interactions cause the relaxation to deviate from eqn (1.4), the temperature dependence usually exhibits a corresponding deviation from Arrhenius behavior (eqn (1.12)). A spectacular increase in the temperature sensitivity of the dynamics is one of the hallmarks of vitrifying liquids and polymers, prototypical of systems with

correlated, multi-body interactions. Understanding the connection between the time and temperature dependences of the dynamics is a major theoretical challenge.

References

1. A. Einstein, *Investigations on the Theory of the Brownian Movement*, (ed. R. Fuerth, translated by A.D. Cowper) Methuen Co., London (1926) and Dover Publ., New York (1956).
2. P. Debye, *Polar Molecules*, Dover, New York (1928).
3. *Rubber & Plastics News*, p. 12, Oct. 20, 2008.
4. J. Meissner, *Rheol. Acta* **10**, 230 (1971).
5. M.H. Wagner and H.M. Laun, *Rheol, Acta* **17**, 138 (1978).
6. C.A. Angell, K.L. Ngai, G.B. McKenna and P.F. McMillan *J. Appl. Phys.* **88**, 3113 (2000).
7. C.M. Roland, S. Hensel-Bielowka, M. Paluch and R. Casalini, *Rep. Prog. Phys.* **68**, 1405 (2005).
8. A.J. Kennedy, *J. Mech. Phys. Solids* **1**, 172 (1953).
9. D. McLean, *Rep. Prog. Phys.* **29**, 1 (1966).
10. T.J. Quinn, C.C. Speake, S.J. Richman, R.S. Davis, and A. Picard, *Phys. Rev. Lett.* **87**, 111101 (2001).
11. P.G. Santangelo and C.M. Roland, *Macromolecules* **31**, 3715 (1998).
12. R. de L. Kronig, *J. Opt. Soc. Am.* **12**, 547 (1926); H.A. Kramers, *Atti del Congresso Internazionale dei Fisici* **2**, 545 (1927).
13. N.W. Tschoegl, *The Phenomenological Theory of Linear Viscoelastic Behavior*, Springer-Verlag, Berlin (1989).
14. M. Wubbenhorst and J. Van Turnhout, *J. Non-Cryst. Sol.* **305**, 40 (2002).
15. Y.I. Shimanskii, *J. Eng. Phys. Thermophys.* **13**, 301 (1967).
16. J.D. Ferry, *Viscoelastic Properties of Polymers*, 3rd edition, Wiley, New York (1980).
17. R. Richert, *J. Non-Cryst. Solids* **172-174**, 209 (1994).
18. R. Kohlrausch Ann. *Phys. Chem. (Poggendorff).* **91**, 179 (1854).
19. G. Williams and D.C. Watts, *Trans. Faraday Soc.* **66**, 80 (1970).
20. C.P. Lindsey and G.D. Patterson, *J. Chem. Phys.* **73**, 3348 (1980).
21. A.K. Jonscher, *J. Mater. Sci.* **16**, 2037 (1981).
22. P.J. Flory, *Proc. Roy. Soc. London* **A234**, 60 (1956).
23. P.J. Flory, *Adv. Polym. Sci.* **59,** 1 (1984).
24. V.G. Baranov, *Fiber Chem.* **9**, 223 (1978).
25. G.K. Elyashevich, *Adv. Polym. Sci.* **43**, 205 (1982).
26. C.M. Roland and M.F. Sonnenschein, *Poly. Eng. Sci.* **31**, 1434 (1991).
27. R. Huisman and H.M. Heuvel, *J. Appl. Polym. Sci.* **37**, 595 (1989).
28. M.J. Schroeder, K.L. Ngai, and C.M. Roland, *J. Polym. Sci. Phys. Ed.* **45** 342 (2007).
29. D.A. McQuarrie, *Statistical Mechanics*, 2nd edition, Chap. 11, University Science Books, Sausalito, CA (2000).
30. C. Kittel, *Quantum Theory of Solids*, 2nd edition, Chap. 19, Wiley, New York (1987).
31. U. Buchenau, M. Prager, N. Nucker, A.J. Dianoux, N. Ahmad, and W.A. Phillips, *Phys. Rev. B* **34**, 5665 (1986).

32. V.K. Malinovsky and A.P. Sokolov. *Solid State Commun.* **57**, 767 (1986).
33. S. Etienne, L. David, A.J. Dianoux, L. Saviot, and E. Duval, *J. Non-Cryst. Sol.* **307–310**, 109 (2002).
34. K.L. Ngai, A. Sokolov, and W. Steffen, *J. Chem. Phys.* **107**, 5268 (1997).
35. G.G. Naumis and H.M. Flores-Ruiz, *Phys. Rev. B* **78**, 094203 (2008).
36. H. Shintani and H. Tanaka, *Nature Mater.* **7**, 870 (2008).
37. C.M. Roland, M.J. Schroeder, J.J. Fontanella and K.L. Ngai, *Macromolecules* **37**, 2630 (2004).
38. S.A. Lusceac, C. Gainaru, M. Vogel, C. Koplin, P. Medick, and E.A. Rössler, *Macromolecules* **38**, 5625 (2005).
39. A.P. Sokolov, A. Kisliuk, V.N. Novikov, and K.L. Ngai, *Phys. Rev. B* **63**, 172204 (2001).
40. G. Caliskan, A. Kisliuk, A.P. Sokolov, and V.N. Novikov, *J. Chem. Phys.* **114**, 10189 (2001); A. Kisliuk, V.N. Novikov, and A.P. Sokolov, *J. Polym. Sci. Polym. Phys. Ed.* **40**, 201 (2002).
41. A. Rivera, A. Leon, C.P.E. Varsamis, A.D. Chryssikos, K.L. Ngai, C.M. Roland, and L.J. Buckley, *Phys. Rev. Lett.* **88**, 125902 (2002).
42. P. Lunkenheimer, A. Pimenov, and A. Loidl, *Phys. Rev. Lett.* **78**, 2995 (1997).
43. R. Casalini, K.L. Ngai, and C.M. Roland, *J. Chem. Phys.* **112**, 5181 (2000).
44. O. Kanert, R. Kuchler, P.C. Soares, and H. Jain, J. Non-Cryst. Sol. **307**, 1031 (2002).
45. A. Burns, G.D. Chryssikos, E. Tombari, R.H. Cole, and W.M. Risen, *Phys. Chem. Glasses* **30**, 264 (1989).
46. H. Cang, V.N. Novikov, and M.D. Fayer, *J. Chem. Phys.* **118**, 2800 (2003).
47. K.L. Ngai, *J. Phys. Condens. Mat*ter **15**, S1107 (2003).
48. C. Gainaru, A. Rivera, S. Putselyk, G. Eska, and E.A. Rössler, *Phys. Rev. B* **72**, 174203 (2005).
49. C. Hansen and R. Richert, *J. Phys. Condens. Matter* **9**, 9661 (1997).
50. C.M. Roland and R. Casalini, *Macromolecules* **40**, 3631 (2007).
51. J. Williams and A. Eisenberg, *Macromolecules* **11**, 700 (1978).
52. Y. Aoki and J.O. Brittain, *J. Appl. Polym. Sci.* **20**, 2879 (1976).
53. S. Corezzi, M. Beiner, H. Huth, K. Schroter, S. Capaccioli, R. Casalini, D. Fioretto, and E. Donth, *J. Chem. Phys.* **117**, 2435 (2002).
54. H.W. Starkweather, *Macromolecules* **14**, 1277 (1981).
55. H.W. Starkweather and J.R. Barkley, *J. Polym. Sci. Polym. Phys. Ed.* **19**, 1211 (1981).
56. O. Yano and Y. Wada, *J. Polym Sci. Polym. Phys. Ed.* **9**, 669 (1971).
57. M. Cook, G. Williams, and T.T. Jones, *Polymer* **16**, 835 (1975).
58. S.S.N. Murthy and M. Shahin, *Eur. Polym. J.* **42**, 715 (2006).
59. B.E. Read and G. Williams, *Polymer* **2**, 239 (1961).
60. K. Adrjanowicz, M. Paluch, and K.L. Ngai, *J. Phys. Condens. Matter* **22**, 125902 (2010).
61. R. Casalini and C.M. Roland, *J. Non-Cryst. Solids*, **357**, 282 (2011).
62. R. Casalini and C.M. Roland, *Phys. Rev. Lett.* **102** 035701 (2009).
63. V.A. Bershstein and V.M. Yegorov, *Polym. Sci. USSR* **27**, 2743 (1985).
64. K.L. Ngai and M. Paluch, *J. Chem. Phys.* **120**, 857 (2004).
65. G.P. Johari and M. Goldstein, *J. Phys. Chem.* **74**, 2034 (1970).
66. K. Schmidt-Rohr, A.S. Kulik, H.W. Beckham, A. Ohlemacher, U. Pawelzik, C. Boeffel, and H.W. Spiess, *Macromolecules* **27**, 4733 (1994).

67. S.C. Kuebler, D.J. Schaefer, C. Boeffel, U. Pawelzik, and H. W. Spiess, *Macromolecules* **30**, 6597 (1997).
68. K.L. Ngai, T.R. Gopalakrishnan, and M. Beiner, *Polymer* **47**, 7222 (2006).
69. G.P. Johari, G. Power and J.K. Vij, *J. Chem. Phys.* **116**, 5908 (2002).
70. K.L. Ngai, *J. Non-Cryst. Sol*ids **351**, 2635 (2005).
71. E. Helfand, *Science* **226**, 647 (1984).
72. I. Bahar, B. Erman, and L. Monnerie, *Macromolecules* **24**, 3618 (1991).
73. P.J. Flory, *J. Am. Chem. Soc.* **67**, 2048 (1945).
74. P.J. Flory, *Ind. Eng. Chem.* **38**, 417 (1946).
75. P.J. Flory, *Chem. Rev.* **35**, 51 (1944).
76. A. Barbieri, D. Prevosto, M. Lucchesi, and D. Leporini, *J. Phys. Condens. Matter* **16**, 6609 (2004).
77. T.G. Fox and P.J. Flory, *J. Polym. Sci.* **14**, 315 (1954).
78. D.T. Turner, *Polymer* **19**, 789 (1978).
79. F. Danusso, M. Levi, G. Gianotti, and S. Turri, *Polymer* **34**, 3687 (1993).
80. K. Ueberreiter and G.J. Kanig, *Colloid Sci.* **7**, 569 (1952).
81. C.G. Robertson and C.M. Roland, J. *Polym. Sci. Polym. Phys. Ed.* **42**, 2604 (2004).
82. A.T. Di Benedetto and L. Di Landro, *J. Polym. Sci.* **27**, 1405 (1989).
83. J.E.L. Roovers and P.M. Toporowski, *J. Appl. Polym. Sci.* **18**, 1685 (1974).
84. K.L. Wooley, C.J. Hawker, J.M. Pochan, and J.M.M. Frechet, *Macromolecules* **26**, 1514 (1993).
85. A. Kisliuk, Y. Ding, J. Hwang, J.S. Lee, B.K. Annis, M.D. Foster, and A.P. Sokolov, *J. Polym. Sci. Polym. Phys. Ed.* **40**, 2431 (2002).
86. J.C. Mitchell and D.J. Meier, *J. Polym. Sci. A2* **6**, 1689 (1968).
87. Z.R. Glaser and F.R. Eirich, *J. Polym. Sci. C* **31**, 275 (1970).
88. G.J. Lake, C.C. Lawrence, and A.G. Thomas, *Rubber Chem. Technol.* **73**, 801 (2000).
89. G. Adam and J.H. Gibbs, *J. Chem. Phys.* **43**, 139 (1965).
90. J.D. Stevenson, J. Schmalian, and P.G. Wolynes, *Nature Phys.* **2**, 268 (2006).
91. H. Sillescu, *J. Non-Cryst. Solids* **243**, 81 (1999).
92. R. Richert, *J. Phys. Condens. Matter* **14**, R703 (2002).
93. L. Berthier, G. Biroli, J.-P. Bouchaud, L. Cipelletti, D. El Masri, D. L'Hote, F. Ladieu, and M. Pierno, *Science* **310**, 1797 (2005).
94. R. Bohmer, G. Diezemann, G. Hinze, and E. Rössler, *Prog. Nucl. Magn. Reson. Spectr.* **39**, 191 (2001).
95. P.G. Santangelo, K.L. Ngai, and C.M. Roland, *Macromolecules* **26**, 2682 (1993).
96. K.L. Ngai and D.J. Plazek *Rubber Chem. Technol.* **68**, 376 (1995).
97. D.J. Plazek, X.D. Zheng, and K.L. Ngai, *Macromolecules* **25**, 4920 (1992).
98. K.L. Ngai, D.J. Plazek, and C.A. Bero, *Macromolecules* **26**, 1065 (1993).
99. D.J. Plazek, I.-C. Chay, K.L. Ngai, and C.M. Roland, *Macromolecules* **28**, 6432 (1995).
100. H. Yamakawa, *Modern Theory of Polymer Solutions*, Harper & Row, New York (1971).
101. B. Erman and J.E. Mark, *Structure and Properties of Rubberlike Networks*, Oxford University Press, Cambridge (1997).
102. O. Johnson, *Information Theory and the Central Limit Theorem*, Imperial College Press, London (2004).
103. P.J. Flory, *Statistical Mechanics of Chain Molecules*, Hanser Publishers, NY (1989).
104. *Polymer Data Handbook*, (ed. J.E. Mark) Oxford University Press, Cambridge (1999).

105. F. Bueche, *J. Chem. Phys.* **20**, 1959 (1952).
106. C.M. Roland, L.A. Archer, P.H. Mott, and J. Sanchez-Reyes, *J. Rheol.* **48**, 395 (2004).
107. L. Harnau, R. G. Winkler, and P. Reineker, *J. Chem. Phys.* **106**, 2469 (1997).
108. R. Faller and F. Müller-Plathe, *Chem. Phys. Chem.* **2**, 180 (2001).
109. M. Bishop, J.H.R. Clarke, A. Rey, and J.J. Freire, *J. Chem. Phys.* **94**, 4009 (1991).
110. D.N. Theodorou and U.W. Suter, *Macromolecules* **18**, 1206 (1985).
111. G. Wei and B.E. Eichinger, *J. Chem. Phys.* **93**, 1430 (1990).
112. T. Minato and A. Hatano, *Macromolecules* **14**, 1035 (1981).
113. G. Wei, *Physica A,* **222**, 155 (1995).
114. S.J. Sciutto, *J. Phys. A: Math. Gen.* **29**, 5455 (1996).
115. C.M. Roland in *The Science and Technology of Rubber*, 3rd edn (eds. J.E. Mark, B. Erman, and F.R. Eirich) Chapter 3, Elsevier, New York (2005).
116. R.P. Quirk and D.L. Gomochak Pickel, in *The Science and Technology of Rubber*, 3rd edition (eds. J.E. Mark, B. Erman, and F.R. Eirich) Chapter 2, Elsevier, New York (2005).
117. G.C. Berry and T.G Fox, *Adv. Polym. Sci.* **5**, 261 (1968).
118. H. Watanabe, T. Sakamoto, and T. Kotaka, *Macromolecules* **18**, 1008 (1995).
119. J.P. Monfort, G. Mann, and P. Monge, *Macromolecules* **17**, 1551 (1984).
120. D.J. Plazek, C. Seoul, and C.A. Bero, *J. Non-Cryst. Solids* **131–133**, 570 (1991).
121. P.-G. de Gennes, *Scaling Concepts in Polymer Physics*, Cornell University, Ithaca (1979).
122. M. Doi and S.F. Edwards, *The Theory of Polymer Dynamics*, Clarendon Press, Oxford (1986).
123. T.P. Lodge, N.A. Rotstein, and S. Prager, *Adv. Chem. Phys.* **79**, 1 (1990).
124. K. Binder, T.P. Lodge, H. Sillescu, K. Schweizer, and H. Yu, *J. Non-Cryst. Solids* **131–133**, 742 (1991).
125. T.C.B. McLeish, *Adv. Phys.* **51**, 1379 (2002).
126. S.-Q. Wang, J. Polym. *Sci. Polym. Phys. Ed.* **41**, 1589 (2003).
127. D.S. Pearson, L.J. Fetters, and W.W. Graessley, *Macromolecules* **27**, 711 (1994).
128. J.F. Vega, S. Rastogi, G.W.M. Peters, and H.E.H. Meijer, *J. Rheol.* **48**, 663 (2004).
129. R.H. Colby, L.J. Fetters, and W.W. Graessley, *Macromolecules* **20**, 2237 (1987).
130. M. Abdel-Goad, W. Pyckhout-Hintzen, S. Kahle, J. Allgaier, D. Richter, and L.J. Fetters, *Macromolecules* **37**, 8135 (2004).
131. I. Muller and P. Strehlow, *Rubber and Rubber Balloons*, Springer, Berlin (2004).
132. E. Verron and G. Marckmann, *Thin-Walled Struc.* **41**, 731 (2003).
133. Y. Levin and F.L. da Silveira, *Phys. Rev. E* **69**, 051108 (2004).
134. H. Nyquist, *Phys. Rev.* **32**, 110 (1928).
135. J.B. Johnson, *Phys. Rev.* **32**, 97 (1928).
136. R. Zwanzig, *Ann. Rev. Phys. Chem.* **16**, 67 (1965).
137. R.G. Gordon, *Adv. Magn. Res.* **3**, 1 (1968).
138. L. Cugliandolo, J. Kurchan, and L. Peliti, *Phys. Rev. E* **55**, 3898 (1997).
139. L. Bellon, S. Ciliberto and C. Laroche, *Eur. Phys. Lett.* **53**, 511 (2001).
140. N. Greinert, T. Wood, and P. Bartlett, *Phys. Rev. Lett.* **97**, 265702 (2006).
141. M.H. Cohen and G.S. Grest, *Phys. Rev. B* **24**, 4091 (1981).
142. R.G. Palmer, D.L. Stein, E. Abrahams and P.W. Anderson, *Phys. Rev. Lett.* **53**, 958 (1984).

143. J.T. Bendler and M.F. Shlesinger, *Macromolecules* **18**, 591 (1985).
144. J. Klafter and A. Blumen, *Chem. Phys. Lett.* **119**, 377 (1985).
145. C. DeDominicis, H. Orland, and F. Lainee, *J. Phys. Lett.* **46**, L463 (1985).
146. P.-G. de Gennes, *Macromolecules* **35**, 3785 (2002).
147. M.N. Berberan-Santos, E.N. Bodunov, and B. Valeur, *Chem. Phys.* **315**, 171 (2005).
148. K.L. Ngai, R.W. Rendell, A.K. Rajagopal, and S. Teitler, *Ann. NY Acad. Sci.* **484**, 150 (1986).
149. M.M. Kubat, P. Riha, R.W. Rychwalski, and S. Uggla, *Mech. Time Dep. Mater.* **3**, 31 (1999).